



Nonlinear Dynamic Inversion based Attitude Control for a Hovering Quad Tiltrotor eVTOL Vehicle

Thomas Lombaerts* John Kaneshige† Stefan Schuet‡ Gordon Hardy§
Bimal Aponso¶ Kimberlee Shish||

NASA Ames Research Center, Moffett Field, CA 94035

Urban Air Mobility is a future mode of transportation that will require a revolutionary new vehicle concept. One of the concepts currently being studied and developed are tiltrotor eVTOL (electrical vertical takeoff and landing) vehicles. One of the many challenges that these vehicles face is manual nonlinear flight control with a focus on minimum required pilot training. This paper discusses a nonlinear dynamic inversion based attitude control law that was designed for this quad tiltrotor vehicle concept. Two advantageous inherent properties of dynamic inversion in this setup are the effective decoupling of the control axes which are by design highly coupled for this kind of vehicle, and its ability to naturally handle changes of operating condition, which removes the need for gain scheduling. These are advantageous for control of tiltrotor VTOL vehicles, due to their wide range of operating conditions which varies from hover to forward flight, and transitioning between them. The inner dynamic inversion control loop, including control allocation to the four rotors, will serve as a core flight control system to which further developments can be naturally added such as autoflight and adaptive flight envelope protection.

Nomenclature

Symbols

α	angle of attack [rad]
β	sideslip angle [rad]
δ_{T_i}	tilt angle of propeller i [rad]
$\delta_{T_{ci}}$	throttle setting [0–1]
η	blending coefficient [0–1]
γ	flight path angle [rad]
ω	angular rate vector [rad/s]
ν	virtual input
ω_n	natural frequency [rad/s]
$\phi/\theta/\psi$	roll / pitch attitude / yaw angle [rad]
ρ	air density [slugs/ft ³]
ζ	damping coefficient [0–1]
\bar{c}	mean aerodynamic chord [ft]

\bar{q}	$= \frac{1}{2}\rho V^2$, dynamic pressure [slugs/(ft s ²)]
\mathcal{M}_{CA}	control efficiencies matrix
\mathbf{F}	force vector [lbs ft/s ²]
\mathbf{f}	nonlinear state function vector
\mathbf{G}	nonlinear function matrix which maps inputs
\mathbf{h}	nonlinear observation function vector
\mathbf{I}	inertia matrix [slugs ft ²]
\mathbf{M}	moment vector [lbs ft ² /s ²]
\mathbf{p}	parameter vector
\mathbf{u}	input vector
\mathbf{V}	speed [kts]
\mathbf{W}	weighting matrix
\mathbf{x}	state vector
\mathbf{y}	output vector
τ_{eng}	engine time constant [s]
b	wingspan [ft]

*Aerospace Research Engineer, Stinger Ghaffarian Technologies, Intelligent Systems Division, Mail Stop 269-1, AIAA Associate Fellow, thomas.lombaerts@nasa.gov

†Computer Engineer, Intelligent Systems Division, Mail Stop 269-1, AIAA member.

‡Computer Engineer, Intelligent Systems Division, Mail Stop 269-3, AIAA member.

§Research Pilot, Science Applications International Corporation, Moffett Field, California 94035, AIAA member.

¶Associate Division Chief, Intelligent Systems Division, Associate Fellow AIAA

||Aerospace Engineer, Intelligent Systems Division, Mail Stop 269-1, AIAA member.

C_D	drag coefficient [-]	n_{prop}	number of rotors
C_L	lift coefficient [-]	$p/q/r$	roll / pitch / yaw rate [rad/s]
C_p	pressure coefficient [-]	RPM	rotations per minute
C_{\bullet}	dimensionless force or moment coefficient [-]	S	wing surface area [ft^2]
c_{T_i}	thrust coefficient of the rotor	T_i	thrust provided by propeller i [lbs]
D_i	rotor diameter [ft]	$X/Y/Z$	force vector components [lbs ft/s^2]
$dx_f/dy_f/dz_f$	location front propeller wrt cg [ft]	0	with respect to trim or previous condition
$dx_r/dy_r/dz_r$	location rear propeller wrt cg [ft]	aero	aerodynamics
F	force [lbs ft/s^2]	BW	bandwidth
g	gravity constant [ft/s^2]	comm	commanded
h	altitude [ft]	fil	filter
I_{\bullet}	scalar for mass inertia [slugs ft^2]	grav	gravity
k_m	torque constant of the propellers	prop	propeller
K_{\bullet}	controller gain	ref	reference
$L/M/N$	moment vector components [$\text{lbs ft}^2/\text{s}^2$]	req	required
m	mass [lbs]	vert	vertical

I. Introduction

RECENTLY, there have been numerous developments in the area of urban air taxi operations, also known as urban air mobility or on-demand mobility applications that help to meet the challenging mobility needs of an increasing population density, taking into account the limited capacity of the currently available transportation infrastructure. One of the enabling technologies of this transportation concept is the vertical take-off and landing (VTOL) capability, where power and energy requirements are minimized by using low disk-loaded rotors, and short range requirements permit consideration of non-traditional propulsion concepts. This is helped by the latest advances in the technological fields of structures, automation and control, scaling of propulsion systems, and energy-storage. The combination of these technologies and capabilities promises to lead to the opportunity to design unconventional new means of transportation, such as urban air mobility with electrical VTOL capability.^{1,2}

Currently, a diverse range of vehicle configurations are being explored, designed and flight tested, such as the Munich based company Lilium with their two-seat Eagle and five-seat Jet, the Airbus subsidiary A³ with the Vahana, the Volocopter VC2, Joby Aviation with the S2 and Lotus, and Kitty Hawk with the Cora, among many others. Although currently not in the design-build-fly phase, the Uber Elevate concept is noteworthy, with their three common reference models (CRM). These are virtual designs which can be used by industry as engineering models for technology development. These vehicles can be divided into three sub-groups, based on the propulsion configuration:

1. tilting propulsion systems: Lilium Eagle and Jet, A³ Vahana, Joby Aviation S2 and Lotus.
2. separate vertical and/or forward propulsion system: Kitty Hawk Cora (both), Uber CRM-002 (both), Uber eCRM-003 (both), Volocopter VC2 (vertical only).
3. separate vertical combined with a tilting propulsion system: Uber eCRM-001, Uber CRM-001.

Another possible grouping is based on ‘winged eVTOL’ versus ‘wingless eVTOL’ designs.

An important advantage of tilting propulsion systems is the flexibility to carry heavier payloads. Also, in case of heavy loading and adverse atmospheric conditions (so-called ‘hot and high’ conditions with lower air density) which prevent a vertical takeoff, the propulsion system can tilt to a certain optimal angle, which would allow for a short takeoff roll.

A. Focus of this paper

This paper will investigate the automation and control challenges that are inherent to this kind of vehicles. Any control system will have to deal with a wide range of flying conditions, varying from hover to forward flight and the transitions between them. Fault tolerance will be a crucial aspect, as well as easy handling and ‘carefree flying’ capability, which will include some kind of envelope protection for upset prevention. Also, the control system setup should allow for manual as well as autoflight control with seamless transitions between both. The lack of detailed model information of these vehicles is an additional robustness challenge that must be taken into account in the control system design.

B. Literature survey

Most control system design literature focuses on the control of quadcopters and other vertical propulsion configurations. Among others, Model Reference Adaptive Control (MRAC) is a popular approach for these applications, in order to deal with large parameter uncertainties.³ Other popular approaches are eigenstructure assignment⁴ and Nonlinear Dynamic Inversion (NDI).⁵ The incremental approach, called incremental nonlinear dynamic inversion (INDI) is beneficial in this kind of application, because this method requires little modeling and is computationally efficient.^{6,7} However, since this approach relies on the so-called time scale separation principle, it is not mathematically rigorous. There is also a lack of stability and robustness analysis for INDI. Therefore, Ref. [8] reformulated the INDI control law without using the time scale separation principle. The stability of the closed-loop system in the presence of external disturbances was analyzed using Lyapunov methods and nonlinear system perturbation theory. Also, the robustness of the closed-loop system against regular and singular perturbations was analyzed. Another familiar constraint of NDI is actuator saturation. Ref. [9] used Incremental Nonlinear Control Allocation to solve this problem for a tailless aircraft with highly coupled control effectors.

Nonlinear Dynamic Inversion is the chosen control approach for the research presented in this paper. This method facilitates the physical interpretation of internal signals. Other important advantages are:

1. Perfect decoupling of the steering channels, which results in a significantly simplified steering task.
2. The control laws are split into a model dependent part and a model independent part. In this way, gain scheduling is not needed.
3. The total control structure involves reference models for command shaping. This is an adequate setup for complying with flying and handling qualities and for incorporating signals that hedge against control saturation as well as envelope protection.

This control setup applied on the class of vehicles studied here, however, is especially prone to control saturation. Therefore, specific protections are needed, such as prioritized control allocation and pseudo control hedging, among others.

C. Paper Structure

The structure of this paper is as follows. The simulation model is described in Sec. II. Sec. III gives an overview of the nonlinear controller and introduces the concepts of nonlinear dynamic inversion (NDI) and incremental NDI (INDI). Then the NDI and INDI control laws are derived for this specific class of vehicle. This section ends with the discussion of the linear controllers and the command filtering and reference models. Initial simulation results are presented in Sec. IV. These results focus primarily on demonstrating the capabilities of the control setup to achieve complete decoupling between the several axes and compensating for aerodynamic transition effects on attitude control at higher airspeeds, for example. Sec. V analyses how this control setup complies with the hover and low speed requirements for small and moderate amplitude attitude changes in the ADS-33 Flying and Handling Qualities requirements. Prioritized control allocation is discussed in Sec. VI since it is an essential feature in this setup to prevent control saturation. Finally, Sec. VII presents the conclusions and recommendations.

II. Simulation Model

A conceptual UAM eVTOL configuration, similar to a Cessna TTx, was used for this concept study. This vehicle has separate lift and cruise rotors, as shown in Fig. 1. A few key characteristics of the vehicle are given in Table 1. The flight mechanics and the propulsion system of the vehicle are described in the remainder of this section.



Figure 1. Illustration of the conceptual vehicle

property	value
mass m	2650 lbs
mass inertia I_{xx}	948 slugs ft ²
mass inertia I_{yy}	1346 slugs ft ²
mass inertia I_{zz}	1967 slugs ft ²
mass inertia I_{xz}	0 slugs ft ² (Ref. [10])
wing area S	174 ft ²
wingspan b	36 ft
capacity	1 pilot + 3 pax
number of lift rotors	4
number of cruise rotors	1

Table 1. Technical specifications of the vehicle

A. Flight Mechanics

The universal kinematic equations for linear and angular accelerations are:

$$\dot{\mathbf{V}} = \frac{1}{m} (\mathbf{F}_{\text{total}} - \boldsymbol{\omega} \times m\mathbf{V}) \quad (1)$$

$$\dot{\boldsymbol{\omega}} = \mathbf{I}^{-1} (\mathbf{M}_{\text{total}} - \boldsymbol{\omega} \times \mathbf{I}\boldsymbol{\omega}) \quad (2)$$

where the total force and moment vectors consist of contributions from aerodynamics, propulsion and gravity:

$$\mathbf{F}_{\text{total}} = \mathbf{F}_{\text{aero}} + \mathbf{F}_{\text{prop}} + \mathbf{F}_{\text{grav}} \quad (3)$$

$$\mathbf{M}_{\text{total}} = \mathbf{M}_{\text{aero}} + \mathbf{M}_{\text{prop}} \quad (4)$$

The aerodynamic contributions are defined by means of their dimensionless coefficients as follows:

$$\mathbf{F}_{\text{aero}} = \begin{bmatrix} X_{\text{aero}} \\ Y_{\text{aero}} \\ Z_{\text{aero}} \end{bmatrix} = \begin{bmatrix} C_X \\ C_Y \\ C_Z \end{bmatrix} \bar{q}S \quad (5)$$

$$\mathbf{M}_{\text{aero}} = \begin{bmatrix} L_{\text{aero}} \\ M_{\text{aero}} \\ N_{\text{aero}} \end{bmatrix} = \begin{bmatrix} bC_l \\ \bar{c}C_m \\ bC_n \end{bmatrix} \bar{q}S \quad (6)$$

where the dimensionless aerodynamic force coefficients are a blending of the conventional lift, drag and sideforce coefficients and the corresponding flat plate coefficients, which is transformed from the aerodynamic

reference frame to the body reference frame:

$$\begin{bmatrix} C_X \\ C_Y \\ C_Z \end{bmatrix} = \begin{bmatrix} \cos \alpha & 0 & -\sin \alpha \\ 0 & 1 & 0 \\ \sin \alpha & 0 & \cos \alpha \end{bmatrix} \begin{bmatrix} \cos \beta & -\sin \beta & 0 \\ \sin \beta & \cos \beta & 0 \\ 0 & 0 & 1 \end{bmatrix} \begin{bmatrix} -C_D \\ -C_Y \\ -C_L \end{bmatrix} \quad (7)$$

$$\begin{bmatrix} C_D \\ C_Y \\ C_L \end{bmatrix} = (1 - \eta_{\text{aero} \rightarrow \text{hover}}) \begin{bmatrix} C_D \\ C_Y \\ C_L \end{bmatrix}_{\text{aero}} + \eta_{\text{aero} \rightarrow \text{hover}} \begin{bmatrix} C_D \\ C_Y \\ C_L \end{bmatrix}_{\text{flat plate}} \quad (8)$$

$$\begin{bmatrix} C_D \\ C_Y \\ C_L \end{bmatrix}_{\text{flat plate}} = \begin{bmatrix} C_p \sin \alpha \cos \beta \\ C_p \sin \beta \\ C_p \sin \alpha \cos \alpha \end{bmatrix} \quad (9)$$

$\eta_{\text{aero} \rightarrow \text{hover}}$ is the blending coefficient between hover and forward flight and varies gradually between 0 and 1 and vice versa during transition phases. This coefficient depends on the airspeed. In full hover $\eta_{\text{aero} \rightarrow \text{hover}}$ is 1 and in pure forward flight it is 0. Eq. (9) is based on conventional aerodynamic modeling of a flat plate, with $C_p = 2$.^{11,12} In a similar way, the blending is applied to the aerodynamic moments, where no flat plate effects are expected on the dimensionless aerodynamic moment coefficients:

$$\begin{bmatrix} C_l \\ C_m \\ C_n \end{bmatrix} = (1 - \eta_{\text{aero} \rightarrow \text{hover}}) \begin{bmatrix} C_l \\ C_m \\ C_n \end{bmatrix}_{\text{aero}} \quad (10)$$

The gravity contribution is:

$$\mathbf{F}_{\text{grav}} = \begin{bmatrix} X_{\text{grav}} \\ Y_{\text{grav}} \\ Z_{\text{grav}} \end{bmatrix} = \begin{bmatrix} -\sin \theta \\ \sin \phi \cos \theta \\ \cos \phi \cos \theta \end{bmatrix} mg \quad (11)$$

The propulsion contributions depend largely on thrust magnitude as well as the tilt angle of the individual nacelles, and the moment arms as defined in Fig. 2:

$$\mathbf{F}_{\text{prop}} = \begin{bmatrix} X_{\text{prop}} \\ Y_{\text{prop}} \\ Z_{\text{prop}} \end{bmatrix} = \begin{bmatrix} \sum_{i=1}^{N_{\text{prop}}} T_i \cos \delta_{T_i} \\ 0 \\ -\sum_{i=1}^{N_{\text{prop}}} T_i \sin \delta_{T_i} \end{bmatrix} \quad (12)$$

$$\mathbf{M}_{\text{prop}} = \begin{bmatrix} L_{\text{prop}} \\ M_{\text{prop}} \\ N_{\text{prop}} \end{bmatrix} = \mathcal{M}_{\text{CA}} \begin{bmatrix} T_1 \\ T_2 \\ T_3 \\ T_4 \end{bmatrix} \quad (13)$$

with:

$$\mathcal{M}_{\text{CA}} = \begin{bmatrix} dy_f \sin \delta_{T_1} - k_m \cos \delta_{T_1} & -dy_f \sin \delta_{T_2} + k_m \cos \delta_{T_2} & dy_r \sin \delta_{T_3} + k_m \cos \delta_{T_3} & -dy_r \sin \delta_{T_4} - k_m \cos \delta_{T_4} \\ dx_f \sin \delta_{T_1} + dz_f \cos \delta_{T_1} & dx_f \sin \delta_{T_2} + dz_f \cos \delta_{T_2} & -dx_r \sin \delta_{T_3} - dz_r \cos \delta_{T_3} & -dx_r \sin \delta_{T_4} - dz_r \cos \delta_{T_4} \\ k_m \sin \delta_{T_1} + dy_f \cos \delta_{T_1} & -k_m \sin \delta_{T_2} - dy_f \cos \delta_{T_2} & -k_m \sin \delta_{T_3} + dy_r \cos \delta_{T_3} & k_m \sin \delta_{T_4} - dy_r \cos \delta_{T_4} \end{bmatrix} \quad (14)$$

In Eq. (14), k_m is the torque constant of the propellers.

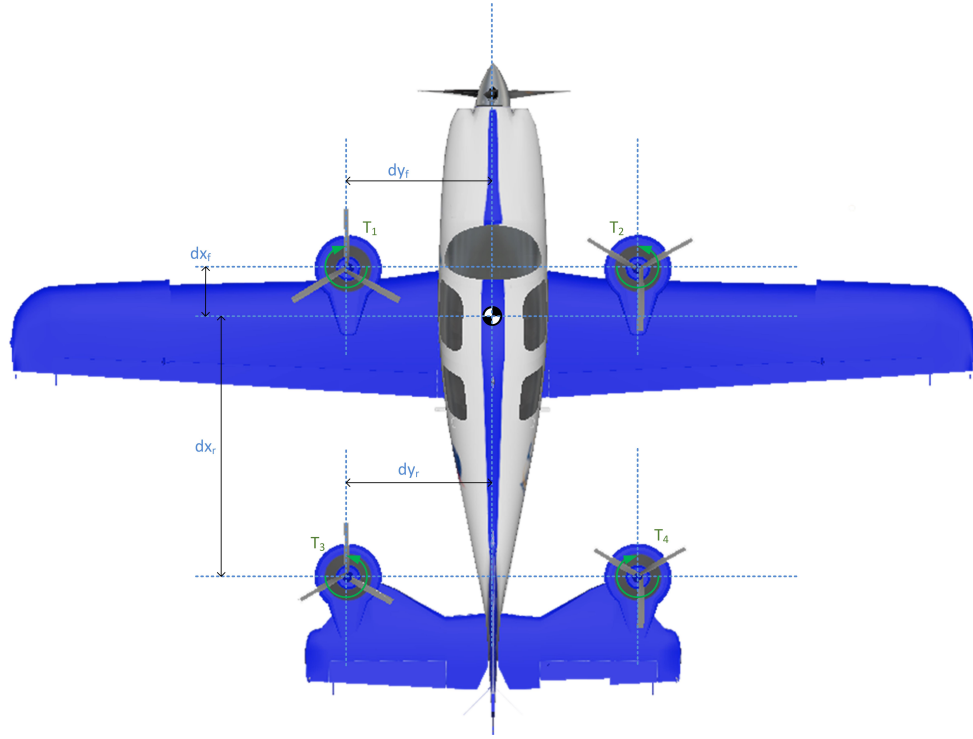


Figure 2. Geometry of the UAM concept model

B. Propulsion system for thrust modeling

The conceptual propulsion system of this vehicle consists of electric motors, and is represented by a simplified model, based on Ref. 13. A few key performance characteristics are given in Table 2. Aerodynamic effects between the rotors and their interaction with the fuselage and wings are currently not modeled. Future work will include more detailed propulsion systems.

characteristic	vertical	cruise
diameter D	2.5 ft	6.5 ft
tilt angle δ_T	90 deg	0 deg
max thrust T_{\max}	1325 lbs	760 lbs
thrust coefficient c_T	0.9	
engine time constant τ_{eng}	1/6 s	

Table 2. Some key performance characteristics per rotor

Since this vehicle is based on RPM control, the throttle setting is translated into a commanded RPM setting, which is limited corresponding to the minimum and maximum thrust values. Subsequently the commanded RPM setting is used for calculating the commanded thrust levels, and the engine dynamics are represented by a first order engine time constant.

The commanded *RPM* value per rotor depends on the throttle setting $\delta_{T_{c_i}}$ which is restricted to the range $[0 - 1]$, within some predefined bounds:

$$RPM_{i,\text{comm}} = \sqrt{\delta_{T_{c_i}}} (RPM_{\max_i} - RPM_{\min_i}) + RPM_{\min_i} \quad (15)$$

Subscript i represents the index of the rotor: $i = 1, 2, \dots, n_{\text{prop}}$ with n_{prop} the total number of rotors. These bounds are based on the maximum and minimum thrust values, which are assumed as known:

$$RPM_{i_{\max}} = \sqrt{\frac{T_{i_{\max}}}{c_{T_i} \rho D_i^6}} \times 60 \quad (16)$$

$$RPM_{i_{\min}} = \sqrt{\frac{T_{i_{\min}}}{c_{T_i} \rho D_i^6}} \times 60 \quad (17)$$

The actual commanded thrust per rotor is then calculated based on the commanded RPM :

$$T_{i_{\text{comm}}} = c_{T_i} \left(\frac{RPM_{i_{\text{comm}}}}{60} \right)^2 \rho D_i^6 \quad (18)$$

The engine dynamics are represented as follows:

$$\dot{T}_i = -\frac{1}{\tau_{\text{eng}}} (T_i - T_{i_{\text{comm}}}) \quad (19)$$

III. Overview of nonlinear controller

The overall controller structure consists of four major modules, namely pilot command filtering for yaw and altitude commands, reference model, the actual controller which contains the dynamic inversion block as well as a linear controller, and envelope estimation, as illustrated in Fig. 3. This general setup is very similar to the setup that was used for a previous flight control project of the first author for a conventional aircraft configuration.¹⁴

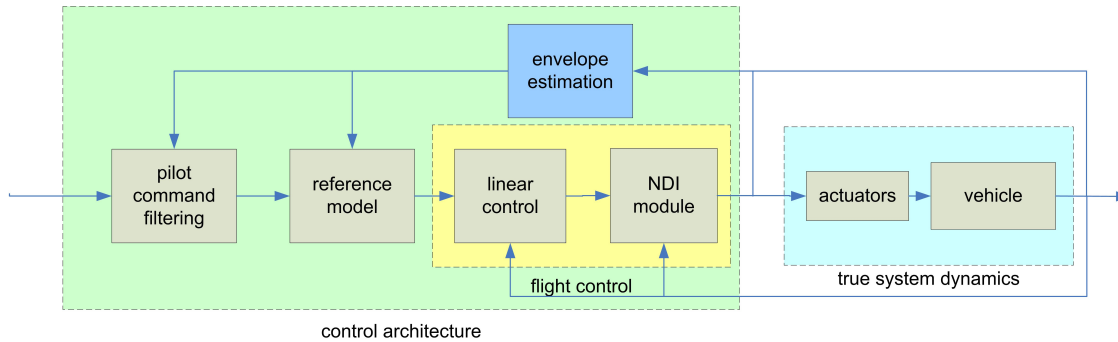


Figure 3. Global overview of the manual control setup

More detail about which quantities are controlled per stage is shown in Fig. 4. The pilot command filtering merely transforms the yaw rate and altitude rate commands, as provided by the pilot through the control inceptors, to commanded values of yaw angle and altitude. This is then combined with the second order reference model. By choosing proper values for natural frequency and damping ratio, the flying qualities requirements are met. Subsequently, the linear controller calculates commanded values of the angular and vertical accelerations, which serve as virtual inputs for the dynamic inversion. The controller gains in this step are purely tuned to optimize reference signal tracking. It should be noted that both aforementioned steps are completely independent of the vehicle. The next two steps involve the actual nonlinear dynamic inversion (NDI) calculation and are dependent of the vehicle. In a first step the dynamics are effectively

inverted and the three required moments and the required vertical force are calculated based on the virtual inputs. This calculation requires the mass and inertia. Finally, the control allocation step maps the required moments and force to required thrust values for each propeller, by using the geometry of the vehicle and the thrust angle of each propeller.

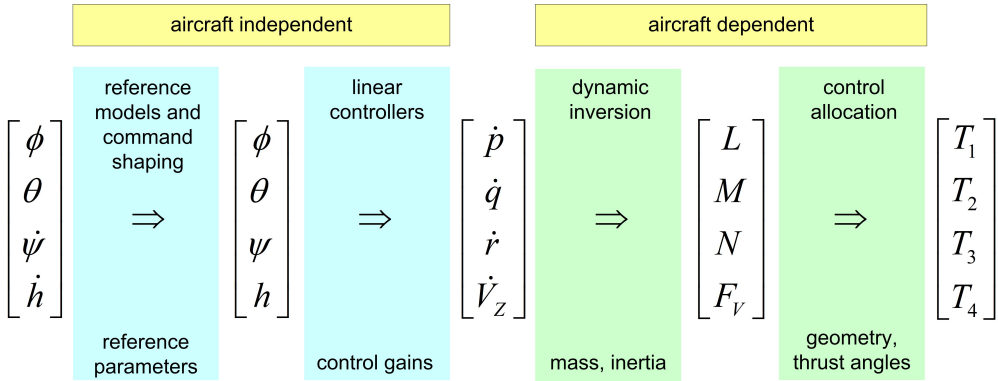


Figure 4. Overview of different control steps and the relevant quantities

A. The concept of nonlinear dynamic inversion

First, the concept of dynamic inversion will be introduced by means of Lie derivatives.

The general idea of nonlinear dynamic inversion is as follows. Consider the nonlinear MIMO system dynamic model, which is assumed to be affine in the input:

$$\dot{\mathbf{x}} = \mathbf{f}(\mathbf{x}, \mathbf{p}) + \mathbf{G}(\mathbf{x}, \mathbf{p})\mathbf{u} \quad (20)$$

The output \mathbf{y} of the system is then expressed as a function \mathbf{h} of the aircraft state vector \mathbf{x} and parameter vector \mathbf{p} :

$$\mathbf{y}(\mathbf{x}) = \mathbf{h}(\mathbf{x}, \mathbf{p}) \quad (21)$$

Defining the matrix $\nabla \mathbf{h}(\mathbf{x})$ as the Jacobian matrix:

$$\frac{\partial \mathbf{h}(\mathbf{x}, \mathbf{p})}{\partial \mathbf{x}} = \nabla \mathbf{h}(\mathbf{x}, \mathbf{p}) \quad (22)$$

the time derivatives of the outputs in eq. (21) can be expressed as:

$$\frac{d\mathbf{y}}{dt} = \nabla \mathbf{h}(\mathbf{x}, \mathbf{p}) [\mathbf{f}(\mathbf{x}, \mathbf{p}) + \mathbf{G}(\mathbf{x}, \mathbf{p})\mathbf{u}] = L_f^1 \mathbf{h}(\mathbf{x}, \mathbf{p}) + L_g \mathbf{h}(\mathbf{x}, \mathbf{p}) \mathbf{u} \quad (23)$$

where $L_f^1 \mathbf{h}(\mathbf{x}, \mathbf{p}) = \nabla \mathbf{h}(\mathbf{x}, \mathbf{p}) \mathbf{f}(\mathbf{x}, \mathbf{p})$ denotes the first order Lie derivative vector and the $L_g \mathbf{h}(\mathbf{x}, \mathbf{p}) = \nabla \mathbf{h}(\mathbf{x}, \mathbf{p}) \mathbf{G}(\mathbf{x}, \mathbf{p})$. If the second term of eq. (23) is zero, more time derivatives of eq. (23) are required, generally until the second term of eq. (23) is nonzero. This nonzero time derivative order is defined as “relative degree”. In general, as the elements within the output vector $\mathbf{y}(\mathbf{x})$ may have different relative degrees, it is convenient to write the time derivative for each output as:

$$\frac{d^{r_i} y_i}{dt^{r_i}} = \frac{d^{r_i} h_i(\mathbf{x}, \mathbf{p})}{dt^{r_i}} = L_f^{r_i} h_i(\mathbf{x}, \mathbf{p}) + \sum_{j=1}^m L_{g_j} L_f^{r_i-1} h_i(\mathbf{x}, \mathbf{p}) u_j \quad (24)$$

In eq. (24), r_i is the relative degree for the i^{th} output. A collection of all differentiated (r_i^{th} order) outputs yields:

$$\mathbf{y}^r(\mathbf{x}) = \mathbf{l}(\mathbf{x}, \mathbf{p}) + \mathbf{M}(\mathbf{x}, \mathbf{p}) \mathbf{u} \quad (25)$$

with:

$$\mathbf{y}^r(\mathbf{x}) = \begin{bmatrix} \frac{d^{r_1} h_1(\mathbf{x})}{dt^{r_1}} \\ \vdots \\ \frac{d^{r_m} h_m(\mathbf{x})}{dt^{r_m}} \end{bmatrix} \quad (26)$$

$$\mathbf{l}(\mathbf{x}, \mathbf{p}) = \begin{bmatrix} L_f^{r_1} h_1(\mathbf{x}, \mathbf{p}) \\ L_f^{r_2} h_2(\mathbf{x}, \mathbf{p}) \\ \vdots \\ L_f^{r_m} h_m(\mathbf{x}, \mathbf{p}) \end{bmatrix} \quad (27)$$

and

$$\mathbf{M}(\mathbf{x}, \mathbf{p}) = \begin{bmatrix} L_{g_1} L_f^{r_1-1} h_1(\mathbf{x}, \mathbf{p}) & L_{g_2} L_f^{r_1-1} h_1(\mathbf{x}, \mathbf{p}) & \cdots & L_{g_m} L_f^{r_1-1} h_1(\mathbf{x}, \mathbf{p}) \\ L_{g_1} L_f^{r_2-1} h_2(\mathbf{x}, \mathbf{p}) & L_{g_2} L_f^{r_2-1} h_2(\mathbf{x}, \mathbf{p}) & \cdots & L_{g_m} L_f^{r_2-1} h_2(\mathbf{x}, \mathbf{p}) \\ \vdots & \vdots & \vdots & \vdots \\ L_{g_1} L_f^{r_m-1} h_m(\mathbf{x}, \mathbf{p}) & L_{g_2} L_f^{r_m-1} h_m(\mathbf{x}, \mathbf{p}) & \cdots & L_{g_m} L_f^{r_m-1} h_m(\mathbf{x}, \mathbf{p}) \end{bmatrix} \quad (28)$$

Solving for \mathbf{u} if the total relative degree $r = r_1 + r_2 + \dots + r_m = n$, with n the number of states of the system, by introducing a virtual outer loop control input vector $\boldsymbol{\nu}$, which consists of time derivatives of control variables $cv_i(\mathbf{x})$ up to the corresponding relative degree r_i :

$$\mathbf{u} = \mathbf{M}^{-1}(\hat{\mathbf{x}}, \hat{\mathbf{p}}) [\boldsymbol{\nu} - \mathbf{l}(\hat{\mathbf{x}}, \hat{\mathbf{p}})] \quad (29)$$

with:

$$\boldsymbol{\nu}(\mathbf{x}) = \begin{bmatrix} \frac{d^{r_1} cv_1(\mathbf{x})}{dt^{r_1}} \\ \vdots \\ \frac{d^{r_m} cv_m(\mathbf{x})}{dt^{r_m}} \end{bmatrix} \quad (30)$$

then this results in a closed-loop system with a linear and decoupled input-output relation:

$$\mathbf{y}^r(\mathbf{x}) = \begin{bmatrix} \frac{d^{r_1} h_1(\mathbf{x})}{dt^{r_1}} \\ \vdots \\ \frac{d^{r_m} h_m(\mathbf{x})}{dt^{r_m}} \end{bmatrix} = \boldsymbol{\nu} = \begin{bmatrix} \frac{d^{r_1} cv_1(\mathbf{x})}{dt^{r_1}} \\ \vdots \\ \frac{d^{r_m} cv_m(\mathbf{x})}{dt^{r_m}} \end{bmatrix} \quad (31)$$

Thus the control law for tracking tasks

$$\frac{d^{r_i} cv_i}{dt^{r_i}} = \frac{d^{r_i} h_{i_d}}{dt^{r_i}} - k_{0_i} e - k_{1_i} \dot{e} - \dots - k_{(r_i-1)_i} e^{(r_i-1)} \quad \text{with } e = y_{i_d}(t) - y_i(t) \quad (32)$$

for $i = 1, \dots, m$ with the k_j 's chosen so that $p^n + k_{n-1}p^{n-1} + \dots + k_1 p$ is a stable polynomial, leads to the exponentially stable tracking dynamics for $i = 1, \dots, m$:

$$e^{(r_i)} + k_{(r_i-1)_i} e^{(r_i-1)} + \dots + k_{1_i} \dot{e} + k_{0_i} e = 0 \quad \text{with } e(t) \rightarrow 0 \quad (33)$$

By making use of Nonlinear Dynamic Inversion (NDI), the nonlinear aircraft dynamics can be canceled out such that the resulting system behaves like a pure single r^{th} order integrator. In eq. (29), $\mathbf{l}(\mathbf{x}, \mathbf{p})$ represents the airframe/engine model and $\mathbf{M}(\mathbf{x}, \mathbf{p})$ is the so-called effector blending model. Note that the effector blending model $\mathbf{M}(\mathbf{x}, \mathbf{p})$ needs to be inverted. More information is available in the literature.^{15,16}

It should be noted that this dynamic inversion is not perfect due to the presence of the multiplicative uncertainties in the aerodynamic model. However, the linear controller has shown to be capable to deal with these modeling errors.

B. The concept of incremental nonlinear dynamic inversion

The incremental form of NDI is based on the computation of the control increment at a given point in time with respect to the condition of the system one incremental time instance in the past.^{6,17-21} Recently, this concept received a lot of attention from the flight control community and was test flown by DLR as early as 2013.

As a first step, the nonlinear system is approximated following a first-order Taylor series expansion of Eq. (20) around the current operating condition in time ‘0’:

$$\dot{\mathbf{x}} \approx \dot{\mathbf{x}}_0 + \frac{\partial}{\partial \mathbf{x}} [\mathbf{f}(\mathbf{x}, \mathbf{p}) + \mathbf{G}(\mathbf{x}, \mathbf{p})\mathbf{u}] \Big|_{\mathbf{x}=\mathbf{x}_0, \mathbf{u}=\mathbf{u}_0} \underbrace{(\mathbf{x} - \mathbf{x}_0)}_{\Delta \mathbf{x}} + \frac{\partial}{\partial \mathbf{u}} [\mathbf{f}(\mathbf{x}, \mathbf{p}) + \mathbf{G}(\mathbf{x}, \mathbf{p})\mathbf{u}] \Big|_{\mathbf{x}=\mathbf{x}_0, \mathbf{u}=\mathbf{u}_0} \underbrace{(\mathbf{u} - \mathbf{u}_0)}_{\Delta \mathbf{u}} \quad (34)$$

The variables with subscript ‘0’ should be interpreted as an incremental time instance before their equivalents without subscript. Observe that several terms in Equation (34) do not depend on either \mathbf{x} or \mathbf{u} . It is assumed that the time-scale separation principle holds. As such, the change in state is considered significantly slower than the change in control input for very small time increments and fast control action ($\mathbf{x} - \mathbf{x}_0 \ll \mathbf{u} - \mathbf{u}_0$). By assuming $\mathbf{x} - \mathbf{x}_0 \approx 0$, Eq. (34) can be simplified as follows:

$$\dot{\mathbf{x}} \simeq \dot{\mathbf{x}}_0 + \mathbf{G}(\mathbf{x}_0, \mathbf{p})\Delta \mathbf{u} \quad (35)$$

The output is required to be set equal to the state ($\mathbf{y} = \mathbf{x}$). Inverting Equation (35) and setting $\nu = \dot{\mathbf{x}}$, the following control law is obtained:

$$\Delta \mathbf{u} \simeq \mathbf{G}(\hat{\mathbf{x}}_0, \hat{\mathbf{p}})^{-1} [\nu - \hat{\mathbf{x}}_0] \quad (36)$$

Note that it is assumed that \mathbf{G} is invertible. The vector $\hat{\mathbf{x}}_0$ contains the state derivatives of inputs computed or estimated from \mathbf{y} or \mathbf{y}_0 , respectively. In the ideal case ($\hat{\mathbf{x}}_0 = \mathbf{x}_0, \hat{\mathbf{x}}_0 = \dot{\mathbf{x}}_0, \hat{\mathbf{p}} = \mathbf{p}$), the input-output response is approximately equal to an integrator. The total input can be obtained by adding the current input \mathbf{u}_0 to the calculated increment:

$$\mathbf{u} = \hat{\mathbf{u}}_0 + \Delta \mathbf{u} \quad (37)$$

The fundamental difference with conventional NDI is that only partial knowledge of the system dynamics is required as the resulting control law only depends on the control effectiveness $\mathbf{G}(\mathbf{x}, \mathbf{p})$. INDI is subsequently less sensitive to model mismatches (i.e. $\hat{\mathbf{p}} \neq \mathbf{p}$), being only dependent on a subset of the uncertain model parameters in \mathbf{p} . However, additional feedback signals are required in the form of state derivatives and the input. In addition, the controller should be discretized with a sufficiently high sampling rate. Finally it should be noted that synchronization between the input and state derivative is required as the calculated control increment is based on a linearisation around a specific operating condition in time.

C. Inner controller core: control allocation

Control allocation calculates the required thrust from the individual propellers in order to achieve certain required moment values:

$$\begin{bmatrix} T_1 \\ T_2 \\ T_3 \\ T_4 \end{bmatrix} = \mathcal{M}_{CA} \backslash \begin{bmatrix} L_{prop} \\ M_{prop} \\ N_{prop} \end{bmatrix} \quad (38)$$

where \backslash represents the left inverse symbol and with:

$$\mathcal{M}_{CA} = \begin{bmatrix} dy_f \sin \delta_{T_1} - k_m \cos \delta_{T_1} & -dy_f \sin \delta_{T_2} + k_m \cos \delta_{T_2} & dy_r \sin \delta_{T_3} + k_m \cos \delta_{T_3} & -dy_r \sin \delta_{T_4} - k_m \cos \delta_{T_4} \\ dx_f \sin \delta_{T_1} + dz_f \cos \delta_{T_1} & dx_f \sin \delta_{T_2} + dz_f \cos \delta_{T_2} & -dx_r \sin \delta_{T_3} - dz_r \cos \delta_{T_3} & -dx_r \sin \delta_{T_4} - dz_r \cos \delta_{T_4} \\ k_m \sin \delta_{T_1} + dy_f \cos \delta_{T_1} & -k_m \sin \delta_{T_2} - dy_f \cos \delta_{T_2} & -k_m \sin \delta_{T_3} + dy_r \cos \delta_{T_3} & k_m \sin \delta_{T_4} - dy_r \cos \delta_{T_4} \end{bmatrix} \quad (39)$$

In Eq. (39), k_m is the torque constant of the propellers.

D. Derivation of the required moments from the required angular accelerations

The total moment is defined as the sum of contributions from propellers and aerodynamics:

$$\mathbf{M}_{\text{tot}} = \mathbf{M}_{\text{prop}} + \mathbf{M}_{\text{aero}} = \mathbf{I}\dot{\omega}_{\text{req}} + \boldsymbol{\omega} \times \mathbf{I}\boldsymbol{\omega} \quad (40)$$

Rewriting to calculate the required moment that must be provided by the propellers:

$$L_{\text{req}} = L_{\text{prop}} = I_{XX}\dot{p}_{\text{req}} - I_{XZ}\dot{r}_{\text{req}} - q(I_{XZp} - I_{ZZr}) - I_{YY}qr - C_{l_{\text{aero}}}\bar{q}Sb \quad (41)$$

$$M_{\text{req}} = M_{\text{prop}} = I_{YY}\dot{q}_{\text{req}} + r(I_{XXq} - I_{XZr}) + p(I_{XZp} - I_{ZZr}) - C_{m_{\text{aero}}}\bar{q}S\bar{c} \quad (42)$$

$$N_{\text{req}} = N_{\text{prop}} = I_{ZZ}\dot{r}_{\text{req}} - I_{XZ}\dot{p}_{\text{req}} - q(I_{XXp} - I_{XZr}) + I_{YY}pq - C_{n_{\text{aero}}}\bar{q}Sb \quad (43)$$

E. Derivation of the required vertical force from the required vertical speed

Newton's second law for the vertical forces:

$$\left(\sum_{i=1}^{N_{\text{prop}}} (T_i \cos(\theta - 90^\circ + \delta_{T_i})) + \left(C_L \frac{1}{2} \rho V^2 S \right) \cos \gamma \right) \cos \phi = m (g + \dot{V}_{Z_{\text{req}}}) \quad (44)$$

Rewriting as the requirement for the vertical component of the total thrust:

$$\sum_{i=1}^{N_{\text{prop}}} (T_i \sin(\theta + \delta_{T_i})) = \frac{m (g + \dot{V}_{Z_{\text{req}}})}{\cos \phi} - \left(C_L \frac{1}{2} \rho V^2 S \right) \cos \gamma \quad (45)$$

Note that $\dot{V}_{Z_{\text{req}}}$ is defined as positive downward.

F. Summary: integrated NDI control for propellers with vertical speed coordination

By combining Eq. (39) and (45), one gets a full rank inversion matrix which takes into account the three moments as well as the vertical force:

$$\begin{bmatrix} T_1 \\ T_2 \\ T_3 \\ T_4 \end{bmatrix} = \mathcal{M}_{\text{CA}_{\text{prop}}}^{-1} \begin{bmatrix} L_{\text{prop}} \\ M_{\text{prop}} \\ N_{\text{prop}} \\ F_{\text{vert req}} \end{bmatrix} \quad (46)$$

with:

$$\mathcal{M}_{\text{CA}_{\text{prop}}} = \begin{bmatrix} dy_f \sin \delta_{T_1} - k_m \cos \delta_{T_1} & -dy_f \sin \delta_{T_2} + k_m \cos \delta_{T_2} & dy_r \sin \delta_{T_3} + k_m \cos \delta_{T_3} & -dy_r \sin \delta_{T_4} - k_m \cos \delta_{T_4} \\ dx_f \sin \delta_{T_1} + dz_f \cos \delta_{T_1} & dx_f \sin \delta_{T_2} + dz_f \cos \delta_{T_2} & -dx_r \sin \delta_{T_3} - dz_r \cos \delta_{T_3} & -dx_r \sin \delta_{T_4} - dz_r \cos \delta_{T_4} \\ k_m \sin \delta_{T_1} + dy_f \cos \delta_{T_1} & -k_m \sin \delta_{T_2} - dy_f \cos \delta_{T_2} & -k_m \sin \delta_{T_3} + dy_r \cos \delta_{T_3} & k_m \sin \delta_{T_4} - dy_r \cos \delta_{T_4} \\ \sin(\theta + \delta_{T_1}) & \sin(\theta + \delta_{T_2}) & \sin(\theta + \delta_{T_3}) & \sin(\theta + \delta_{T_4}) \end{bmatrix} \quad (47)$$

Besides the required moments and forces in Eq. (46) are calculated as follows:

$$\begin{bmatrix} L_{\text{prop}} \\ M_{\text{prop}} \\ N_{\text{prop}} \\ F_{\text{vertreq}} \end{bmatrix} = \begin{bmatrix} I_{XX}\dot{p}_{\text{req}} - I_{XZ}\dot{r}_{\text{req}} - q(I_{XZp} - I_{ZZr}) - I_{YY}qr & -C_{l_{\text{aero}}}\bar{q}Sb \\ I_{YY}\dot{q}_{\text{req}} + r(I_{XXq} - I_{XZr}) + p(I_{XZp} - I_{ZZr}) & -C_{m_{\text{aero}}}\bar{q}S\bar{c} \\ I_{ZZ}\dot{r}_{\text{req}} - I_{XZ}\dot{p}_{\text{req}} - q(I_{XXp} - I_{XZr}) + I_{YY}pq & -C_{n_{\text{aero}}}\bar{q}Sb \\ \frac{m(g + \dot{V}_{Z_{\text{req}}})}{\cos \phi} - (C_L \bar{q}S) \cos \gamma \end{bmatrix} \quad (48)$$

G. Alternative: integrated INDI control for propellers with vertical speed coordination

Based on the principles of Incremental NDI, as outlined in Sec. B, the equation for the required moments and forces (48) in Sec. F can be rewritten and simplified.

Starting with the dynamic equation that describes the required angular acceleration, as derived from Eq. (40):

$$\dot{\omega}_{\text{req}} = \mathbf{I}^{-1} \left[\underbrace{\mathcal{M}_{\text{CA}} \cdot \mathbf{T} + \mathbf{M}_{\text{aero}} - \omega \times \mathbf{I}\omega}_{\mathbf{M}_{\text{prop}}} \right] \quad (49)$$

Linearizing this equation with first order Taylor expansions for ω and \mathbf{T} results in the following expression:

$$\begin{aligned} \dot{\omega}_{\text{req}} \approx & \mathbf{I}^{-1} [\mathcal{M}_{\text{CA}} \cdot \mathbf{T}_0 + \mathbf{M}_{\text{aero}_0} - \omega_0 \times \mathbf{I}\omega_0] + \\ & \frac{\partial}{\partial \omega} [\mathbf{I}^{-1} [\mathbf{M}_{\text{aero}} - \omega \times \mathbf{I}\omega]] \Big|_{\omega=\omega_0, \mathbf{T}=\mathbf{T}_0} (\omega - \omega_0) + \\ & \frac{\partial}{\partial \mathbf{T}} [\mathbf{I}^{-1} [\mathcal{M}_{\text{CA}} \cdot \mathbf{T}]] \Big|_{\omega=\omega_0, \mathbf{T}=\mathbf{T}_0} (\mathbf{T} - \mathbf{T}_0) \end{aligned} \quad (50)$$

Defining the previous time step as:

$$\dot{\omega}_0 = \mathbf{I}^{-1} [\mathcal{M}_{\text{CA}} \cdot \mathbf{T}_0 + \mathbf{M}_{\text{aero}_0} - \omega_0 \times \mathbf{I}\omega_0] \quad (51)$$

Implementing Eq. (51) in Eq. (50) and simplifying for the assumption that $(\omega - \omega_0) \ll (\mathbf{T} - \mathbf{T}_0)$ for small time steps:

$$\begin{aligned} \dot{\omega}_{\text{req}} \approx & \dot{\omega}_0 + \frac{\partial}{\partial \mathbf{T}} [\mathbf{I}^{-1} [\mathcal{M}_{\text{CA}} \cdot \mathbf{T}]] \Big|_{\omega=\omega_0, \mathbf{T}=\mathbf{T}_0} (\mathbf{T} - \mathbf{T}_0) \\ \approx & \dot{\omega}_0 + \mathbf{I}^{-1} \mathcal{M}_{\text{CA}} \cdot \mathbf{dT} \quad \text{with : } \mathbf{dT} = \mathbf{T} - \mathbf{T}_0 \end{aligned} \quad (52)$$

Finally, rewriting for the actual control input based on the previous input and the incremental control input:

$$\mathbf{T} = \mathbf{T}_0 + \mathbf{dT} \quad \text{with : } \mathbf{dT} = \mathcal{M}_{\text{CA}}^{-1} \mathbf{I} (\dot{\omega}_{\text{req}} - \dot{\omega}_0) \quad (53)$$

Similarly, for the vertical speed coordination one can start from Eq. (45) and rewrite for the required vertical acceleration:

$$m\dot{V}_{Z_{\text{req}}} = \sum_{i=1}^{N_{\text{prop}}} (T_i \sin(\theta + \delta_{T_i})) \cos \phi + (C_L \bar{q} S) \cos \gamma \cos \phi - mg \quad (54)$$

Linearizing this equation around $m\dot{V}_{Z_0}$ with first order Taylor expansions for T_i , and assuming time scale separation as previously, results in the following expression:

$$m\dot{V}_{Z_{\text{req}}} \approx m\dot{V}_{Z_0} + \frac{\partial}{\partial \mathbf{T}} \left(\sum_{i=1}^{N_{\text{prop}}} (T_i \sin(\theta + \delta_{T_i})) \cos \phi \right) \Big|_{T_i=T_{i0}} (\mathbf{T} - \mathbf{T}_0) \quad (55)$$

Which can be rewritten as:

$$m\dot{V}_{Z_{\text{req}}} \approx m\dot{V}_{Z_0} + \cos \phi \begin{bmatrix} \sin(\theta + \delta_{T_1}) & \dots & \sin(\theta + \delta_{T_{N_{\text{prop}}}}) \end{bmatrix} \cdot \mathbf{dT} \quad \text{with : } \mathbf{dT} = \mathbf{T} - \mathbf{T}_0 \quad (56)$$

Rewriting for the actual control input based on the previous input and the incremental control input:

$$\mathbf{T} = \mathbf{T}_0 + \mathbf{dT} \quad \text{with : } \mathbf{dT} = \begin{bmatrix} \sin(\theta + \delta_{T_1}) & \dots & \sin(\theta + \delta_{T_{N_{\text{prop}}}}) \end{bmatrix} \setminus \frac{m}{\cos \phi} (\dot{V}_{Z_{\text{req}}} - \dot{V}_{Z_0}) \quad (57)$$

Summarizing, combining Eq. (53) and (57) results in the overall INDI control law:

$$\mathbf{T} = \hat{\mathbf{T}}_0 + \mathbf{dT} \quad \text{with : } \mathbf{dT} = \mathcal{M}_{\text{CA}_{\text{prop}}}^{-1} \begin{bmatrix} \mathbf{I}(\dot{\omega}_{\text{req}} - \hat{\omega}_0) \\ \frac{m}{\cos \phi} (\dot{V}_{Z_{\text{req}}} - \hat{V}_{Z_0}) \end{bmatrix} \quad (58)$$

Or:

$$\begin{bmatrix} T_1 \\ T_2 \\ T_3 \\ T_4 \end{bmatrix} = \begin{bmatrix} \hat{T}_{1_0} \\ \hat{T}_{2_0} \\ \hat{T}_{3_0} \\ \hat{T}_{4_0} \end{bmatrix} + \begin{bmatrix} dT_1 \\ dT_2 \\ dT_3 \\ dT_4 \end{bmatrix} \quad \text{with : } \begin{bmatrix} dT_1 \\ dT_2 \\ dT_3 \\ dT_4 \end{bmatrix} = \mathcal{M}_{\text{CA}_{\text{prop}}}^{-1} \begin{bmatrix} I_{XX} (\dot{p}_{\text{req}} - \hat{p}_0) - I_{XZ} (\dot{r}_{\text{req}} - \hat{r}_0) \\ I_{YY} (\dot{q}_{\text{req}} - \hat{q}_0) \\ I_{ZZ} (\dot{r}_{\text{req}} - \hat{r}_0) - I_{XZ} (\dot{p}_{\text{req}} - \hat{p}_0) \\ \frac{m}{\cos \phi} (\dot{V}_{Z_{\text{req}}} - \hat{V}_{Z_0}) \end{bmatrix} \quad (59)$$

with:

$$\mathcal{M}_{\text{CA}_{\text{prop}}} = \begin{bmatrix} dy_f \sin \delta_{T_1} - k_m \cos \delta_{T_1} & -dy_f \sin \delta_{T_2} + k_m \cos \delta_{T_2} & dy_r \sin \delta_{T_3} + k_m \cos \delta_{T_3} & -dy_r \sin \delta_{T_4} - k_m \cos \delta_{T_4} \\ dx_f \sin \delta_{T_1} + dz_f \cos \delta_{T_1} & dx_f \sin \delta_{T_2} + dz_f \cos \delta_{T_2} & -dx_r \sin \delta_{T_3} - dz_r \cos \delta_{T_3} & -dx_r \sin \delta_{T_4} - dz_r \cos \delta_{T_4} \\ k_m \sin \delta_{T_1} + dy_f \cos \delta_{T_1} & -k_m \sin \delta_{T_2} - dy_f \cos \delta_{T_2} & -k_m \sin \delta_{T_3} + dy_r \cos \delta_{T_3} & k_m \sin \delta_{T_4} - dy_r \cos \delta_{T_4} \\ \sin(\theta + \delta_{T_1}) & \sin(\theta + \delta_{T_2}) & \sin(\theta + \delta_{T_3}) & \sin(\theta + \delta_{T_4}) \end{bmatrix} \quad (60)$$

By comparing Eq. (59) with (46) and (48), one can see that for INDI only mass and inertial properties are needed, together with the geometry and torque constant for the control allocation matrix. However, no aerodynamic properties are needed for INDI in the hover phase, contrary to the conventional NDI approach. This is a significant advantage for the class of vehicles as studied in this paper, because it is assumed that no detailed aerodynamic information of these vehicles will be available.

An important aspect of INDI, however, is the need for filtered signals for previous control commands as well as the state derivatives. The angular accelerations are acquired via differentiating and filtering of the angular rates. Filtering is required to limit the noise due to differentiation. The filter is of a second-order low-pass form:

$$H_{\text{fil}}(s) = \frac{\omega_{n_{\text{fil}}}^2}{s^2 + 2\zeta_{\text{fil}}\omega_{n_{\text{fil}}}s + \omega_{n_{\text{fil}}}^2} \quad (61)$$

The same filter is applied on the measurement or model output of the previous control input. Note that care should be taken with selecting the filter coefficients. The estimated angular accelerations should be sufficiently free of noise such that subsequent noise propagation into the control laws is avoided. Noisy control signals can lead to excessive wear on the actuators and increased likelihood of failure. The filter bandwidth $\omega_{n_{\text{fil}}}$ could be lowered to 80 rad/s before serious performance degradation was observed (especially for compensating for aerodynamic transition effects). The damping ratio ζ_{fil} was set equal to 1.

H. Linear controllers

Because of the relative degree, the linear controllers work up to the second order time derivative, and they have the following control law:

$$\nu_p = \dot{p}_{\text{req}} = K_\phi (\phi_c - \phi) + K_{\dot{\phi}} (\dot{\phi}_c - \dot{\phi}) + K_{\ddot{\phi}} (\ddot{\phi}_c) \quad (62)$$

$$\nu_q = \dot{q}_{\text{req}} = K_\theta (\theta_c - \theta) + K_{\dot{\theta}} (\dot{\theta}_c - \dot{\theta}) + K_{\ddot{\theta}} (\ddot{\theta}_c) \quad (63)$$

$$\nu_r = \dot{r}_{\text{req}} = K_\psi (\psi_c - \psi) + K_{\dot{\psi}} (\dot{\psi}_c - \dot{\psi}) + K_{\ddot{\psi}} (\ddot{\psi}_c) \quad (64)$$

The values of the controller gains mentioned in Eq. (62)–(64) are specified in Table 3. The first and second order time derivatives of the control commands used in Eq. (62)–(64) are fed forward internal signals

from the second order reference models discussed in Sec. I. In general, for manual control, integral action is sometimes added in the first term of these linear control laws, if needed.¹⁴ However, this was not necessary in this specific control setup. In future work, additional TRC (translational rate command) outer loops will be added around these loops, which makes integral action at this level undesirable.

Table 3. Linear controller gains for Eq. (62)–(64)

axis	angle	rate	acceleration
roll & pitch	$K_{\phi/\theta} = 5$	$K_{\dot{\phi}/\dot{\theta}} = 5$	$K_{\ddot{\phi}/\ddot{\theta}} = 1$
yaw	$K_{\psi} = 6$	$K_{\dot{\psi}} = 5$	$K_{\ddot{\psi}} = 1$

I. Command filtering and reference model

The reference models for all three channels are of the second order:

$$H_{\text{ref}}(s) = \frac{\omega_{n_{\text{ref}}}^2}{s^2 + 2\zeta_{\text{ref}}\omega_{n_{\text{ref}}}s + \omega_{n_{\text{ref}}}^2} \quad (65)$$

The parameter values for Eq. (65) are defined in Table 4 and were chosen such that the reference model satisfies the ADS-33 Flying and Handling Quality requirements, as discussed in Sec. V. There is a fine balance in choosing the optimal frequency, taking into account the ADS-33 requirements on one hand and the engine time constant on the other hand. Faster (smaller) engine time constants allow for faster reference frequencies, which makes it easier to satisfy the requirements. Slower (larger) engine time constants place an upper limit on the reference frequencies, which makes it impossible to satisfy the ADS-33 requirements. Furthermore, these reference models will be instrumental for future work, which will include pseudo control hedging^{22–24} and safe flight envelope protections.^{25–28} Both previously developed techniques must be adapted for this class of vehicle.

Table 4. Reference model parameters

axis	damping ratio	natural frequency
roll & pitch	$\zeta_{\phi/\theta} = 0.8$	$\omega_{n_{\phi/\theta}} = 2.4 \text{ rad/s}$
yaw	$\zeta_{\psi} = 0.8$	$\omega_{n_{\psi}} = 4.8 \text{ rad/s}$

For the yaw and the altitude steering channels, additional command filtering is needed, involving an integrator, such that both become rate command heading/altitude hold modes.¹⁴

J. Overview of the closed loop system

Fig. 5 shows the detailed overview how all the previously discussed blocks are interconnected in the closed loop system. The aircraft model currently studied in this paper involves only differential thrust control over the four propellers for attitude control in hover and low speed flight, as illustrated in Fig. 5. However, future work will extend to higher speed forward flight. This will require more control inputs for the aerodynamic control surfaces and their actuators. The model inversion and control allocation blocks in Fig. 5 are specified by Eq. (48) (NDI model inversion) or Eq. (59) (INDI model inversion) and Eq. (60) (control allocation). These modules are the only airframe dependent part of the overall control law, where values for the mass, inertia, geometry, thrust angles, torque coefficient and aero (NDI only) parameters are needed. The linear control module in Fig. 5 is specified by Eq. (62)–(64) and the reference model is defined in Eq. (65). Both are airframe independent, but flying and handling qualities dependent. The reference model parameters in Eq. (65) are tuned for satisfying the ADS-33 flying and handling quality requirements, and the linear controller parameters in Eq. (62)–(64) are tuned for reference signal tracking. This decoupled control setup simplifies

controller parameter tuning significantly. Fig. 5 also shows the feedforward channels for reference angular rates and accelerations from reference model to linear controller, further simplifying signal handling.

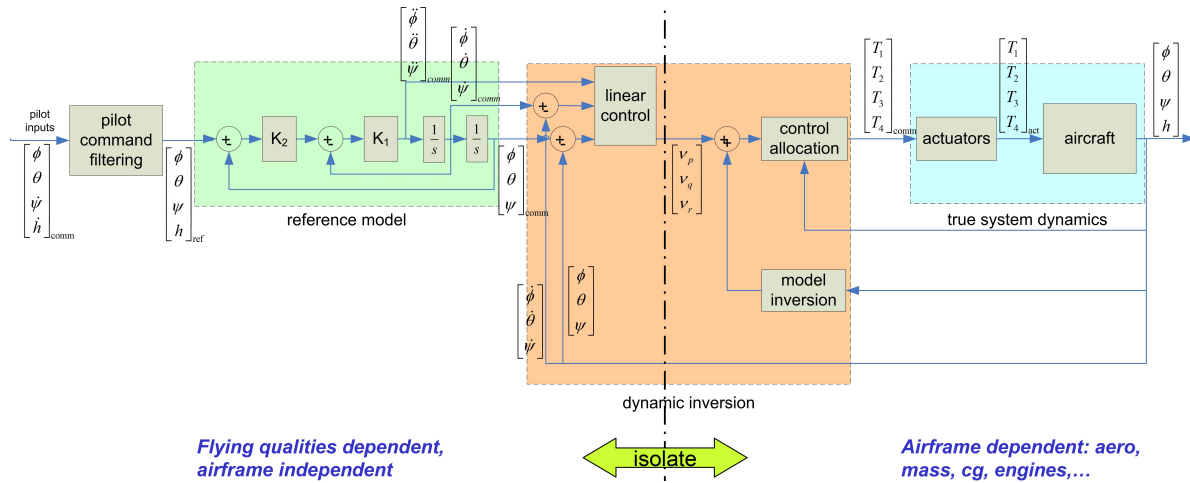


Figure 5. Detailed overview of the control structure and interconnections

IV. Simulation results of the nonlinear controller

This section discusses the performance of the nonlinear hover controller for the decoupling between axes, compensating thrust levels for tilting rotors as well as for compensating for aerodynamic transition effects on attitude control. These aerodynamic effects become significant at higher airspeeds. The simulations results as shown below are all generated with the INDI controller, unless stated otherwise.

A. Decoupling between axes

Fig. 6 shows the controller performance for an overlapping sequence of step commands on all three different axes for pitch, roll and yaw rate. First the vehicle pitches 5 deg nose down, thereafter it rolls 5 deg to the right, and then makes a 24 deg heading change. Finally, it rolls the wings back to level and pitches back up to the initial attitude of 0 deg. Fig. 6(a) shows the commands and responses for roll, pitch and yaw angles, it shows excellent decoupling between the three axes. Only a very minor impact of heading change is visible on roll and pitch attitude angle. Fig. 6(b) shows the body angular rates. Note that these are defined in the body reference frame, where the previous angles in Fig. 6(a) are defined in the inertial reference frame. One can observe non-zero body roll and pitch rates for a non-zero yaw rate. This is intentional instead of a coupling effect, because of the Euler equations. As an example for the yaw rate: $\dot{\psi} = q \frac{\sin \phi}{\cos \theta} + r \frac{\cos \phi}{\cos \theta}$. Fig. 6(c) shows the commands and responses of the required moments that must be provided by the propellers, as calculated in Eq. (41)–(43). The control allocation part of the nonlinear controller, defined in Eq. (38) and (39), calculates the required thrust that each rotor must provide, shown in Fig. 6(d) in order to achieve the required moments, shown in Fig. 6(c). Due to the geometry of the vehicle as outlined in Fig. 2, one can see that the thrust actions per propeller are pairwise anti-symmetric depending on the controlled axis. For pitch commands, $T_1 - T_2$ and $T_3 - T_4$ are pairwise symmetric. For roll commands, this applies to $T_1 - T_3$ and $T_2 - T_4$ and finally $T_1 - T_4$ and $T_2 - T_3$ for yaw.

B. Thrust level compensation for tilting rotors

Since the control allocation part of the flight controller via Eq. (60) takes the tilt angles of the individual rotors δ_{T_i} for $i = 1, \dots, N_{\text{prop}}$ into account, the required thrust levels are automatically compensated for

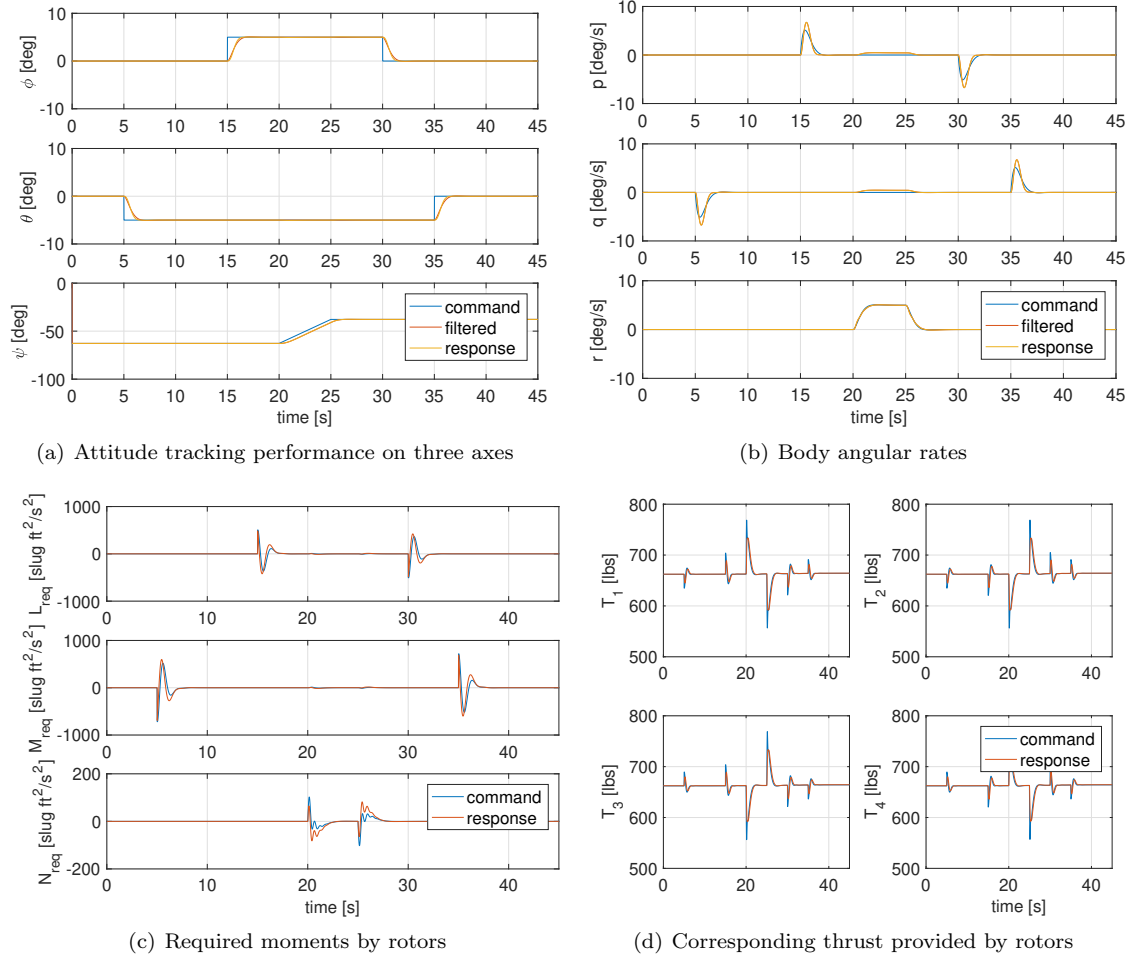


Figure 6. Decoupling performance of the attitude controller for an overlapping sequence of commands

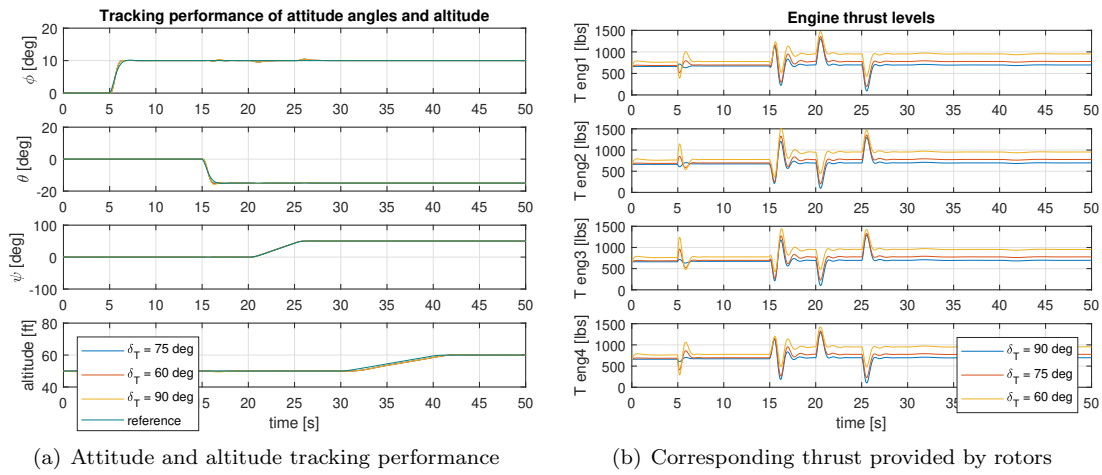


Figure 7. Comparison of thrust level compensation for tilting rotors at $\delta_T = 90, 75$ and 60 deg

tilting rotors. However, for larger tilt angles it becomes more likely that the maximum thrust limit will be reached during maneuvers. The concept vehicle studied here has no tilting rotors, but 4 fixed vertical and 1 cruise rotor, see also Fig. 1. However, an engineering and development model with tiltrotors was developed for analyzing the thrust level compensation capabilities of the controller. Fig. 7 compares the different thrust levels for some basic maneuvers with rotor tilt angles at 90 (vertical), 75 and 60 deg.

C. Transition aerodynamic effects on attitude control at higher airspeeds

Fig. 8 illustrates how aerodynamic transition effects on attitude control are compensated for in the case of regular NDI control. This becomes especially relevant during forward flight at higher speeds, as illustrated in this specific case study. Fig. 8(a) shows that the vehicle pitches 10 deg down, the net total thrust vector of the propellers tilts forward and the vehicle starts to speed up at a constant pace between 5s and 40s. As soon as the vehicle exceeds 30 knots forward airspeed, the wings start to generate aerodynamic effects, such as the aerodynamic pitching moment $C_{m\text{aero}}$ shown here which builds up between 20s and 40s. Subsequently, by means of Eq. (42), the required pitching moment M_{req} is adjusted accordingly to compensate for this aerodynamic effect, shown in the lowest subplot of Fig. 8(a) between 20s and 40s. Finally, the control allocation part of the nonlinear controller, defined in Eq. (38) and (39), calculates the required thrust that each rotor must provide to achieve this compensating pitching moment M_{req} . Fig. 8(b) shows that the individual thrust actions per propeller are again pairwise anti-symmetric for the forward propellers $T_1 - T_2$ and the rear $T_3 - T_4$. The compensation for the aerodynamic transition effects appears again between 20s and 40s.

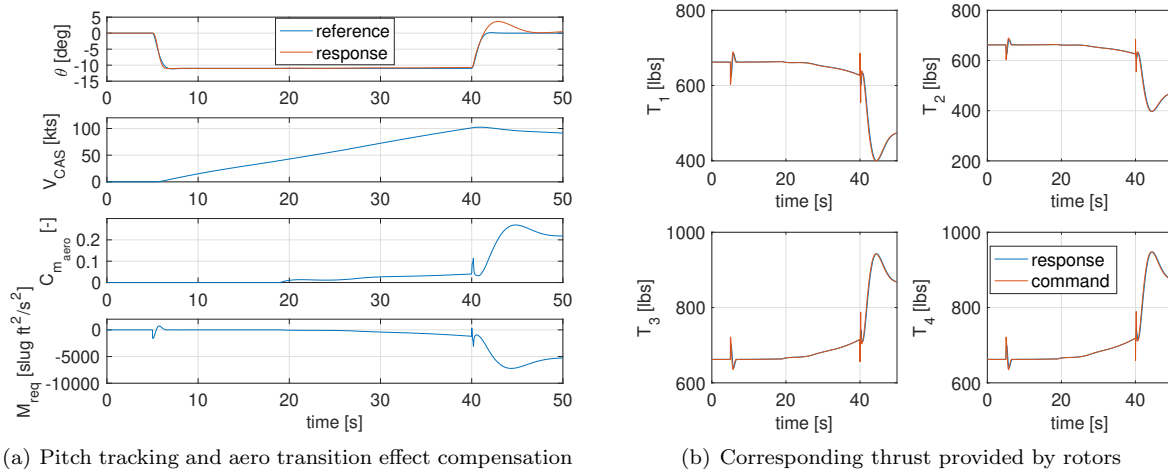


Figure 8. Aero transition effect compensation of the NDI attitude controller for high speed forward flight

Fig. 9 shows a similar case study of compensating control action for aerodynamic transition effects, here for the incremental NDI based approach for attitude control. A similar trend in the aerodynamic pitching moment coefficient $C_{m\text{aero}}$ results in similar compensating behavior of the incremental required pitching moment ΔM_{req} , which is much smaller in magnitude but consistent with the observations in Fig. 8(a). The thrust action by the propellers for the INDI approach, shown in Fig. 9(b), is very similar to the situation for the NDI approach shown in Fig. 8(b). For the control action shown in Fig. 8(b) however, detailed model information about $C_{m\text{aero}}$ is needed for the full inversion in Eq. (42). The control action shown in Fig. 9(b) does not need this model information and relies on the (second order low pass filtered) body pitch acceleration $\dot{\hat{q}}$ instead, via $\dot{M}_{\text{req}} = I_{YY}(\dot{q}_{\text{req}} - \dot{\hat{q}}_0)$, elaborated in Eq. (59).

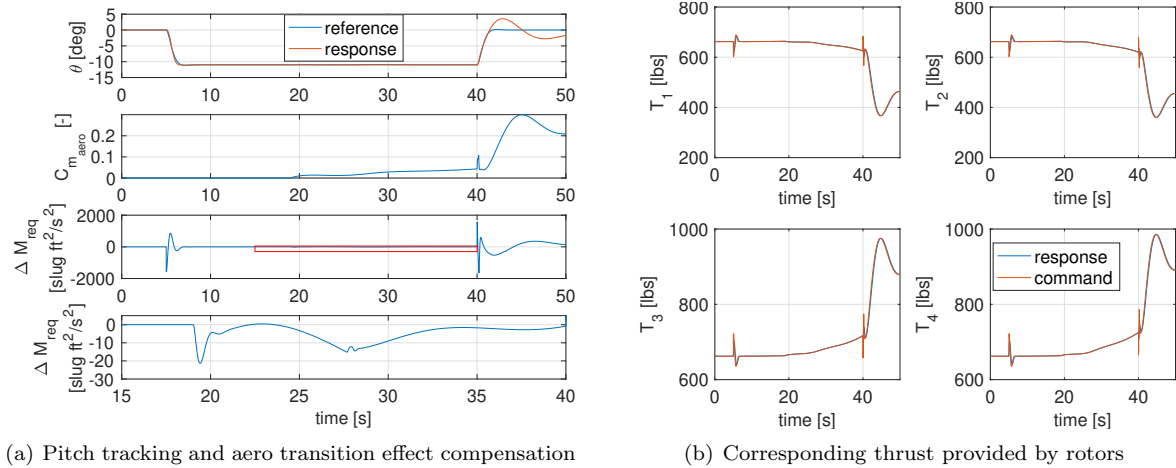


Figure 9. Aero transition effect compensation of the INDI attitude controller for high speed forward flight

V. Compliance with Flying and Handling Qualities Requirements: ADS-33

For this study, the ADS-33 Flying and Handling Qualities Requirements²⁹ were used as a tool to evaluate the performance of the vehicle. This certification document mentions a wide range of requirements for a variety of flight conditions. In this paper, focus is placed on the hover and low speed requirements for small and moderate amplitude changes.

All ADS-33 requirements depend on the applicable Mission-Task-Elements (MTE) and Usable Cue Environment (UCE). These two parameters define how strict the requirements are. For the analysis presented here, which is a case study of a utility vehicle for passenger operations, all MTE's except target acquisition and tracking are considered, and $UCE > 1$. More background information on MTE's and UCE is given in Ref. [29, 30].

Compliance with the ADS-33 requirements depends on the control settings but also on the hardware constraints, such as maximum thrust level T_{max} and especially the engine time constant τ_{eng} . This time constant determines the maximum frequency value in the reference model $\omega_{n_{ref}}$, and this value has an important influence on the performance, and whether the ADS-33 requirements are satisfied, as shown in Table 5.

Table 5. Influence of engine time constant on the performance and compliance with the ADS-33 requirements

τ_{eng}	max $\omega_{n_{ref}}$		ADS-33	margin to bounds
	θ / ϕ	ψ		
1/3 s	1.4 rad/s	2.0 rad/s	level 2	-
1/5 s	2.0 rad/s	4.0 rad/s	level 1	marginal
$\leq 1/6$ s	2.4 rad/s	4.8 rad/s	level 1	significant margin

A. Hover and low speed requirements for small-amplitude attitude changes

For the hover and low speed requirements for small amplitude pitch and roll attitude changes requirements, the short-term response to control inputs was considered. The ADS-33 requirements provide well-defined limits for the pitch and roll response to longitudinal and lateral cockpit control position inputs respectively, as shown in Fig. 10(b) for pitch and Fig. 10(d) for roll. The bandwidth ω_{BW} and phase delay τ_p parameters

are obtained from the corresponding frequency responses shown in Fig. 10(a) for pitch and Fig. 10(c) for roll. For this specific controller design, frequency sweeps were applied as reference signals on the pilot's control inceptors for the closed loop system. For pitch as well as roll, the command amplitude was 20 deg, and the frequency range varied from $\omega_{\min} = 10^{-3}$ to $\omega_{\max} = 10^3$. This ensured sufficient excitation in the reference signal as well as system response, such that an accurate transfer function and Bode plot could be estimated from the time histories. Since the response types for longitudinal and lateral control inputs are 'Attitude Command Attitude Hold' (ACAH), Ref. [29] mentions that the bandwidth depends on the phase diagram only: $\omega_{\text{BW}} = \omega_{\text{BW}_{\text{phase}}}$, which is the 135 deg phase lag crossover frequency: $\omega_{\text{BW}_{\text{phase}}} = \omega_{\Phi=135\text{deg}}$. Besides, Ref. [29] cautions that for ACAH, if $\omega_{\text{BW}_{\text{gain}}} < \omega_{\text{BW}_{\text{phase}}}$, or if $\omega_{\text{BW}_{\text{gain}}}$ is indeterminate, the vehicle may be PIO (Pilot Induced Oscillation) prone for super-precision tasks or aggressive pilot technique. Here the bandwidth for the gain is defined as:

$$\omega_{\text{BW}_{\text{gain}}} = \omega \left(\left| \frac{\theta}{\theta_i} \right| = \left| \frac{\theta}{\theta_i} (\omega_{\Phi=180\text{deg}}) \right| + 6\text{dB} \right) \quad (66)$$

Finally the phase delay τ_p was determined from the slope of the linear least squares fit to the phase curve between ω_{180} and $2\omega_{180}$.

Fig. 10(a) and 10(c) show how bandwidth and phase delay were determined for pitch and roll respectively. These were determined for the reference models, with the reference parameters defined in Sec. III.I, which are plotted in red in the Bode plots, as well as for the actual closed loop systems, plotted in blue in the Bode plots. For the actual closed loop systems, bandwidth and phase delay were calculated for four different engine time constants: $\tau_{\text{motor}} = 1/3, 1/5, 1/6$ and $1/9$ s. All these values are marked in the requirements regions shown in Fig. 10(b) for pitch and Fig. 10(d) for roll. The hover and low speed requirements are satisfied for all engine time constants except $\tau_{\text{motor}} = 1/3$ s, for pitch as well as for roll. In general, a faster time constant results in closed loop performance that gets closer to the reference model.

Similar calculations were done for yaw, but they were slightly different since the pedals control the yaw rate $\dot{\psi}$ instead of the angle, resulting in slightly different requirements for the bandwidth:

$$\omega_{\text{BW}} = \min(\omega_{\text{BW}_{\text{gain}}}; \omega_{\text{BW}_{\text{phase}}}) \quad (67)$$

Fig. 10(e) shows that in the yaw channel, because of the rate control setup, the magnitude diagram of the Bode plot exhibits a 20 dB per decade steeper slope and the phase diagram exhibits an extra 90 deg of phase lag. Fig. 10(f) shows similar results as for pitch and roll. The closed loop system satisfies the requirements for all engine time constants except $\tau_{\text{motor}} = 1/3$ s.

Another important requirement for small-amplitude pitch and roll attitude changes, applies to the mid-term response to control inputs. Any oscillatory mode following an abrupt controller input shall have an effective damping ratio of at least $\zeta \geq 0.35$. The effective damping ratio is related to the magnitude peak in the Bode plot, by means of the following equation for $0 \leq \zeta \leq \sqrt{2}/2$:

$$\zeta = \sqrt{\frac{1}{2} \left(1 - \sqrt{1 - \left(\left| \frac{\theta}{\theta_i} (j\omega) \right|_{\max} \right)^{-1}} \right)} \quad (68)$$

The results of these calculations for the aforementioned engine time constants are presented in Table 6 and show that the minimum effective damping ratio is met for all values except $\tau_{\text{motor}} = 1/3$ s in roll.

B. Hover and low speed requirements for moderate amplitude attitude changes

The hover and low speed requirements for moderate amplitude pitch, roll and yaw attitude changes consider the ratio of peak pitch, roll and yaw rate to change in pitch and roll attitude and heading change, also called attitude quickness. $q_{\text{pk}}/\Delta\theta_{\text{pk}}$, $p_{\text{pk}}/\Delta\phi_{\text{pk}}$ and $r_{\text{pk}}/\Delta\psi_{\text{pk}}$ must meet the limits specified in Fig. 11(b), 11(c) and 11(d) respectively. The required attitude and heading changes must be made as rapidly as possible from one steady attitude and heading to another. The time histories in Fig. 11(a) show the pulses (20° for θ , ϕ and 40° for ψ) on the inputs and the time responses. The corresponding attitude quickness ratios are plotted in Fig. 11(b), 11(c) and 11(d), which show that all requirements are met, except for $\tau_{\text{motor}} = 1/3$ s in roll.

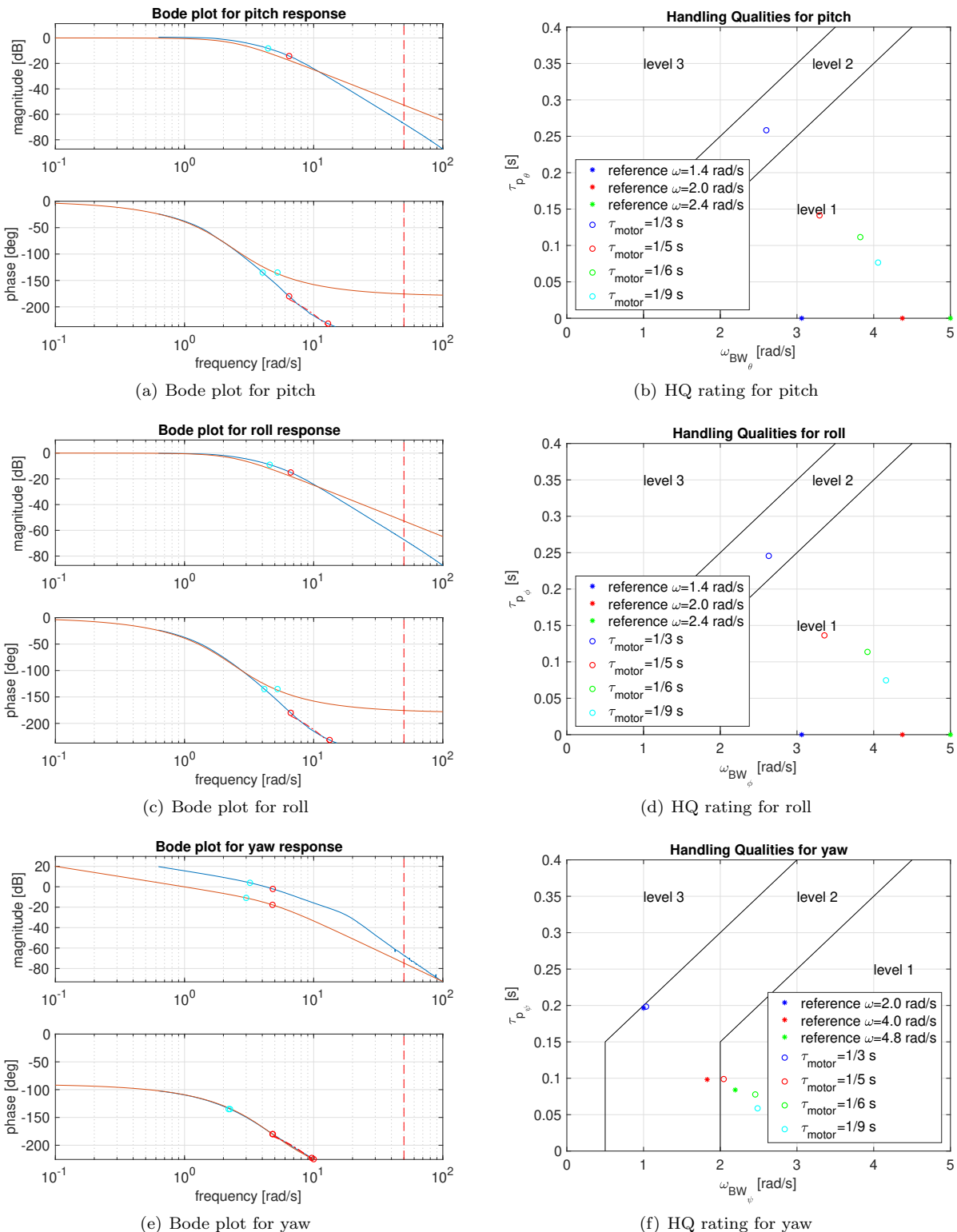
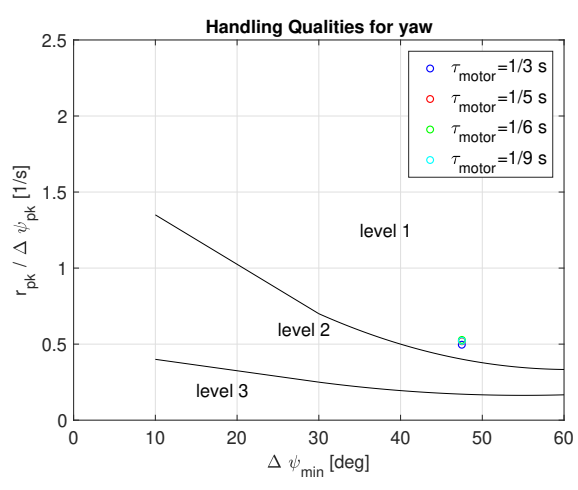
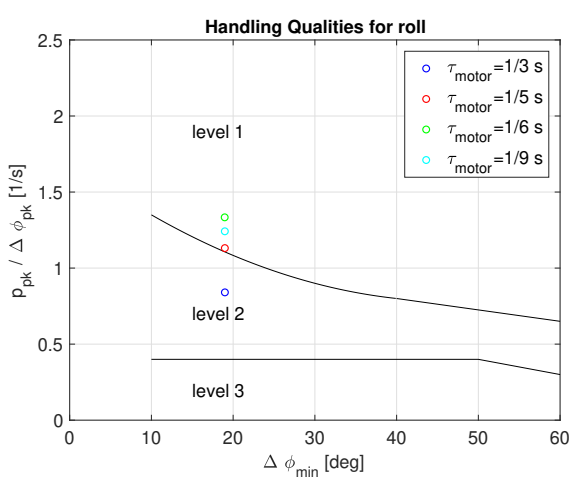
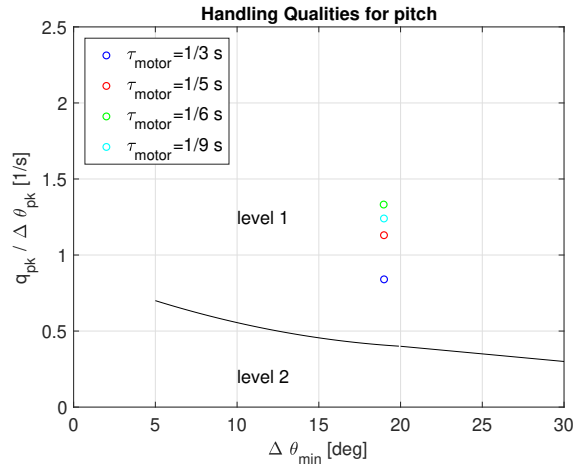
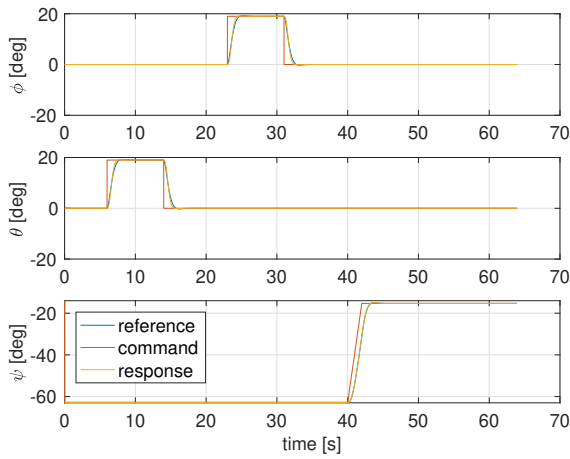


Figure 10. Compliance with hover and low speed requirements for small-amplitude attitude changes

Table 6. Effective damping ratio for pitch and roll for different motor time constants

τ_{motor}	1/3 s		1/5 s		1/6 s		1/9 s	
	ζ	$\geq 0.35?$						
pitch	0.50	✓	0.54	✓	0.55	✓	0.55	✓
roll	0.30	✗	0.40	✓	0.45	✓	0.46	✓

**Figure 11. Compliance with hover and low speed requirements for moderate-amplitude attitude changes**

VI. Prioritized Control Allocation

As briefly introduced earlier, thrust control saturation is a crucial constraint in this control setup. Especially for aerial vehicles with coupled control effectors, such as this vehicle, actuator saturation may lead to undesired and even catastrophic behavior. With the unprioritized control allocation scheme as given in Eq. (60), it may be that the desired combination of pitching, rolling and yawing moment together with vertical force is not achievable due to maximum or minimum thrust limitations of the propellers. In absence of an adequate control allocation algorithm, it is left to chance which one (or combination) of the four objectives will be affected. However, for the flight stability of these multirotor vehicles, it is crucial to apply the full required pitch and roll moments before anything else.³¹ Thereafter, the vertical force for altitude control comes in the second place, followed by the yawing moment which is the least essential from a safety point of view. Therefore, a control allocation algorithm is needed that prioritizes the control objectives of roll and pitch over altitude, and subsequently over yaw, and that calculates the required thrust levels per rotor accordingly. Multiple control allocation algorithms have been proposed, some of which do not adequately address prioritization: ganging, redistributed pseudo-inverse, direct control allocation. Others do address prioritization, such as linear programming and quadratic programming.³² This paper considers a quadratic cost function, and the corresponding quadratic optimization problem. A solution to this problem can be found in a straightforward way using the active set method, as shown by Ref. [33].

In this paper, the Weighted Least Squares (WLS) control allocation algorithm is integrated into the aforementioned dynamic inversion based attitude and altitude controller. This chosen control allocation algorithm solves the weighted, bounded least-squares problem by means of the cost function that makes a trade off between the actual input commands \mathbf{u} and the virtual commands ν :

$$\min \|\mathbf{W}_u(\mathbf{u} - \mathbf{u}_d)\|^2 + \gamma \|\mathbf{W}_\nu(\mathbf{B}\mathbf{u} - \nu)\|^2 \quad (69)$$

subject to: $\mathbf{u}_{\min} \leq \mathbf{u} \leq \mathbf{u}_{\max}$, where \mathbf{B} is the control effectiveness matrix, ν is the commanded virtual control, \mathbf{u}_{\min} and \mathbf{u}_{\max} are the lower and upper position limits, \mathbf{W}_ν is the virtual control weighting matrix, \mathbf{W}_u is the control weighting matrix, \mathbf{u}_d is the desired control and finally γ is the weighting between the relative importance of actual control \mathbf{u} and virtual control ν in the overall cost function.

This problem was solved using an active set method.³³ For this specific vehicle, the highest priority should be given to pitch and roll, followed by altitude and finally yaw.³¹ As a consequence, the relevant weighting matrix \mathbf{W}_ν is defined as: $\mathbf{W}_\nu = \text{diag}(1000, 1000, 1, 100)$. The virtual control inputs are $\nu_{\text{NDI}} = [L_{\text{req}} \ M_{\text{req}} \ N_{\text{req}} \ F_{\text{vert req}}]^T$ for NDI and $\nu_{\text{INDI}} = [\dot{L}_{\text{req}} \ \dot{M}_{\text{req}} \ \dot{N}_{\text{req}} \ \dot{F}_{\text{vert req}}]^T$ for INDI. The control inputs are $\mathbf{u} = [T_1 \ T_2 \ T_3 \ T_4]^T$. The control effectiveness matrix is $\mathbf{B} = \mathcal{M}_{\text{CA}_{\text{prop}}}$, see Eq. (60). Scalar weight $\gamma = 10^{-6}$, desired control inputs $\mathbf{u}_d = \mathbf{0}$ and control weighting matrix $\mathbf{W}_u = \text{diag}(1, 1, 1, 1)$, which are default settings for this algorithm.

A proof of concept example of this prioritized control allocation algorithm is shown in Fig. 12. This figure shows the closed loop system performance for a series of step inputs on roll and pitch, followed by two ramp inputs on yaw and altitude, all well separated over time. The maximum thrust for all rotors was artificially limited for this example to 800 lbs in order to highlight the difference with and without prioritization. Figures 12(a) and 12(c) show tracking performance and the corresponding thrust levels without prioritization. These figures show that thrust saturation occurs frequently throughout the combined maneuver, and this has a major impact on all tracked variables. Figures 12(b) and 12(d) show similar graphs with prioritization, allowing for a back to back comparison. These figures show that, despite thrust saturation, the tracking performance is better. Tracking of pitch and roll is much better. The altitude tracking is significantly improved as well. All these improvements come at the expense of a deteriorated performance in yaw tracking, consistent with the purpose of the prioritized control allocation strategy.

Table 7 shows some RMS values of the tracking error per steering channel and per control allocation strategy, which quantify the tracking performance. These metrics confirm the observations in Fig. 12 that prioritized control allocation by means of weighted least squares improves tracking performance where it is needed most. Depending on the thrust limitations in practice, a more balanced trade off in the prioritization might be necessary.

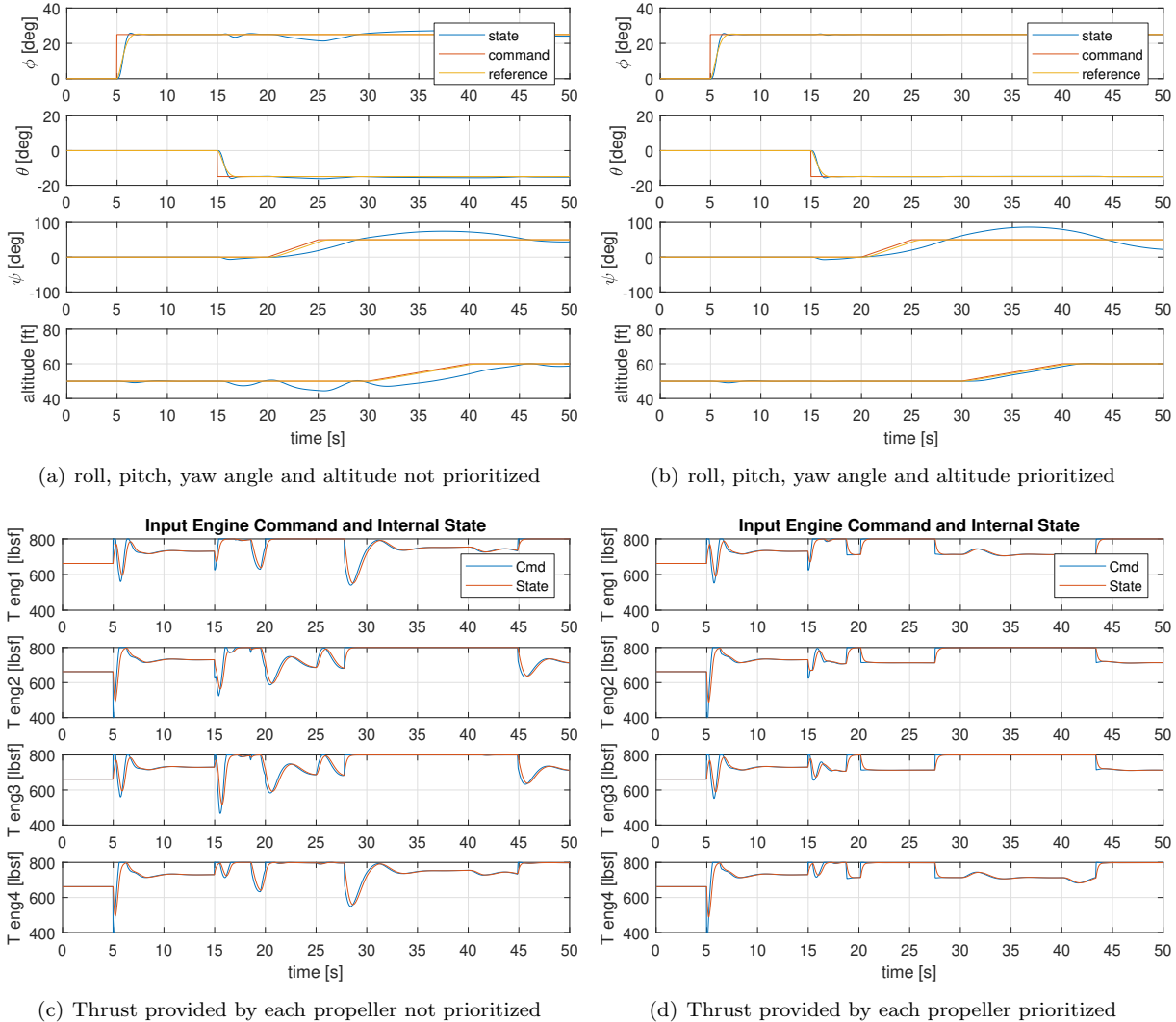


Figure 12. States and inputs comparison with and without prioritization

Table 7. Tracking metrics of reference signals with and without prioritization

Not prioritized	Prioritized
RMS $\phi = 1.5098$ deg	RMS $\phi = 0.39169$ deg
RMS $\theta = 0.53908$ deg	RMS $\theta = 0.2587$ deg
RMS $\psi = 12.6343$ deg	RMS $\psi = 17.4046$ deg
RMS altitude = 2.9781 ft	RMS altitude = 0.47315 ft

VII. Conclusions and recommendations

In this research, nonlinear dynamic inversion (NDI) as well as incremental nonlinear dynamic inversion (INDI) was applied for integrated attitude/altitude control of a quad tiltrotor eVTOL vehicle for hover conditions. Both approaches have the following advantages: (1.) Perfect decoupling of the steering channels, which results in a significantly simplified steering task. (2.) The control laws are split in an airframe dependent part and an airframe independent part. In this way, gain scheduling is not needed. (3.) The total control structure involves reference models for command shaping. This is a good method for complying with flying and handling qualities and for incorporating of future planned functionalities in the control setup. (4) Internal flight control states have a physical meaning and are interpretable. INDI has the additional advantage that it is less dependent on aerodynamic modeling parameters, as shown by the transition analysis of the attitude controller for aerodynamic effects at higher airspeeds. This is particularly useful for eVTOL UAM vehicles, since it is expected that the available aerodynamic modeling information of these vehicles will be limited. Analysis indicated that the closed loop performance satisfies all ADS-33 handling qualities requirements in hover and low speed for small and moderate amplitude attitude changes, as long as the engine time constant is smaller than the threshold $\tau_{eng} \leq 1/5$. Prioritized control allocation by means of weighted least squares was successfully implemented and evaluated in a proof of concept simulation.

This flight control design resulted in an overall closed loop system with satisfactory performance that can serve as a baseline for further evaluations. One of the first next steps is expanding the functional envelope of the controller to include forward flight and the most challenging phase of transitioning back and forth between hover and forward flight. The Weighted Least Squares Control Allocation strategy must extend to include the aerodynamic control surfaces which are to be used at higher airspeeds. Pseudo control hedging and safe flight envelope protection limits must be added to the reference models in this control setup and fault tolerance to certain failures, such as a rotor failure, must be analyzed. Finally, the command filtering as part of the pilot control interface needs to transition seamlessly between configurations for hover and forward flight. Hover involves Attitude Control Attitude Hold (ACAH) for pitch and roll angles, Rate Control Heading Hold (RCHH) for yaw and Rate Control Altitude Hold (RCAH) for altitude. Forward flight, on the other hand, is defined by rate control attitude hold (RCAH) for flight path angle and roll angle and Attitude Control Attitude Hold (ACAH) for sideslip.

Acknowledgments

The authors would like to thank Joe Totah for his support and expert advice in developing the propulsion simulation model as described in Sec. II.B. Also a special thanks to Carlos Malpica and Shannah Withrow for their support in developing new simulation models for this category of eVTOL vehicles through the RVLT project, which will be used in the next project phase.

References

- ¹Swartz, K. I., "Charging Forward - New eVTOL Concepts Advance," *Vertiflite*, July - August 2017.
²Johnson, W., Silva, C., and Solis, R., "Concept Vehicles for VTOL Air Taxi Operations," *AHS Technical Conference on Aeromechanics Design for Transformative Vertical Flight*, January 2018.

- ³Achtelik, M., Bierling, T., Wang, J., Höcht, L., and Holzapfel, F., "Adaptive Control of a Quadcopter in the Presence of large/complete Parameter Uncertainties," *AIAA Infotech@Aerospace*, No. AIAA 2011-1485, American Institute of Aeronautics and Astronautics AIAA, 2011.
- ⁴Yanguo, S. and Huanjin, W., "Design of Flight Control System for a Small Unmanned Tilt Rotor Aircraft," *Chinese Journal of Aeronautics*, Vol. 22, No. 3, jun 2009, pp. 250–256, DOI: 10.1016/S1000-9361(08)60095-3.
- ⁵Francesco, G. D. and Mattei, M., "Modeling and Incremental Nonlinear Dynamic Inversion Control of a Novel Unmanned Tiltrotor," *Journal of Aircraft*, Vol. 53, No. 1, jan 2016, pp. 73–86, DOI: 10.2514/1.C033183.
- ⁶Sieberling, S., Chu, Q. P., and Mulder, J. A., "Robust Flight Control Using Incremental Nonlinear Dynamic Inversion and Angular Acceleration Prediction," *Journal of Guidance, Control, and Dynamics*, Vol. 33, No. 6, nov 2010, pp. 1732–1742.
- ⁷Smeur, E., de Croon, C., and Chu, Q., "Cascaded Incremental Nonlinear Dynamic Inversion Control for MAV Disturbance Rejection," *Control Engineering Practice*, Vol. 73, April 2018, pp. 79–90.
- ⁸Wang, X., van Kampen, E.-J., Chu, Q., and Lu, P., "Stability Analysis for Incremental Nonlinear Dynamic Inversion Control," *AIAA SciTech Forum*, No. AIAA-2018-1115, American Institute of Aeronautics and Astronautics, Jan. 2018, DOI: 10.2514/6.2018-1115.
- ⁹Matamoros, I. and de Visser, C. C., "Incremental Nonlinear Control Allocation for a Tailless Aircraft with Innovative Control Effectors," *2018 AIAA Guidance, Navigation, and Control Conference*, No. AIAA-2018-1116, American Institute of Aeronautics and Astronautics, jan 2018, DOI: 10.2514/6.2018-1116.
- ¹⁰Roskam, J., *Airplane Flight Dynamics and Automatic Flight Controls*, chap. Stability and Control Derivatives for a small general aviation airplane such as the Cessna 182, DARcorporation, 1995, pp. 480 – 486.
- ¹¹Hoerner, S. F. and Borst, H. V., *Fluid-Dynamic Lift, Practical Information on Aerodynamic and Hydrodynamic Lift*, Mrs. Liselotte A. Hoerner, 1985.
- ¹²Hoerner, S. F., *Fluid-Dynamic Drag, Practical Information on Aerodynamic Drag and Hydrodynamic Resistance*, Sighard F. Hoerner, 1965.
- ¹³Totah, J. J., "Mathematical Model of a Tiltwing Aircraft," *47th Annual Forum of the Amecian Helicopter Society*, May 1991.
- ¹⁴Lombaerts, T. and Looye, G., "Design and flight testing of manual nonlinear flight control laws," *AIAA Guidance, Navigation and Control Conference*, No. AIAA 2011-6469, 2011, DOI: 10.2514/6.2011-6469.
- ¹⁵Chu, Q., *Lecture Notes AE4-394, Modern Flight Test Technologies and System Identification*, Delft University of Technology, Faculty of Aerospace Engineering, 2007.
- ¹⁶Slotine, J.-J. E. and Li, W., *Applied Nonlinear Control*, Prentice Hall, 1991.
- ¹⁷Grondman, F., Looye, G., Kuchar, R. O., Chu, Q. P., and Kampen, E.-J. V., "Design and Flight Testing of Incremental Nonlinear Dynamic Inversion-based Control Laws for a Passenger Aircraft," *2018 AIAA Guidance, Navigation, and Control Conference*, American Institute of Aeronautics and Astronautics, jan 2018.
- ¹⁸van Ekeren, W., Looye, G., Kuchar, R. O., Chu, Q. P., and Kampen, E.-J. V., "Design, Implementation and Flight-Tests of Incremental Nonlinear Flight Control Methods," *2018 AIAA Guidance, Navigation, and Control Conference*, American Institute of Aeronautics and Astronautics, jan 2018.
- ¹⁹Pollack, T., Looye, G., and van der Linden F.L.J., "Design and flight testing of flight control laws integrating incremental nonlinear dynamic inversion and servo current control," *AIAA SciTech Conference*, American Institute of Aeronautics and Astronautics, 2019.
- ²⁰Keijzer, T., Looye, G., Chu, Q., and van Kampen, E.-J., "Design and Flight Testing of Incremental Backstepping based Control Laws with Angular Accelerometer Feedback," *AIAA SciTech Conference*, 2019.
- ²¹Zhang, Y. and Jiang, J., "Bibliographical review on reconfigurable fault-tolerant control systems," *Annual Reviews in Control*, Vol. 36, No. 5, jun 2008, pp. 257–268.
- ²²Johnson, E. N. and Calise, A. J., "pseudo-control hedging: a new method for adaptive control," *Advances in Navigation Guidance and Control Technology Workshop*, 2000, Available at: soliton.ae.gatech.edu/people/ejohnson/ngct-paper-johnson.pdf.
- ²³Holzapfel, F., "Dynamic Inversion Based Control Concept with Application to an Unmanned Aerial Vehicle," *AIAA Guidance, Navigation, and Control Conference and Exhibit*, No. AIAA-2004-4907, 2004.
- ²⁴Lombaerts, T., Looye, G., Chu, Q., and Mulder, J., "Pseudo Control Hedging and its Application for Safe Flight Envelope Protection," *AIAA Guidance, Navigation and Control Conference*, No. AIAA 2010-8280, August 2010, DOI: 10.2514/6.2010-8280.
- ²⁵Lombaerts, T., Schuet, S., Wheeler, K., Acosta, D., and Kaneshige, J., "Safe Maneuvering Envelope Estimation based on a Physical Approach," *AIAA Guidance, Navigation and Control (GNC) Conference*, No. AIAA-2013-4618, August 2013, DOI: 10.2514/6.2013-4618.
- ²⁶Schuet, S., Lombaerts, T., Acosta, D., Wheeler, K., and Kaneshige, J., "Autonomous Flight Envelope Estimation for Loss-of-Control Prevention," *Journal of Guidance, Control and Dynamics*, , No. AIAA 2014-0268, 2016, DOI: 10.2514/1.g001729.
- ²⁷Lombaerts, T., Looye, G., Ellerbroek, J., and Rodriguez y Martin, M., "Design and Piloted Simulator Evaluation of Adaptive Safe Flight Envelope Protection Algorithm," *Journal of Guidance, Control and Dynamics*, 2017, DOI: 10.2514/1.G002525.
- ²⁸Lombaerts, T., Looye, G., Seefried, A., Neves, M., and Bellmann, T., "Proof of concept simulator demonstration of a physics based self-preserving flight envelope protection algorithm," *Engineering Applications of Artificial Intelligence*, Vol. 67, jan 2018, pp. 368–380, DOI: 10.1016/j.engappai.2017.08.014.

²⁹ “Aeronautical Design Standard, Performance Specification, Handling Qualities Requirements for Military Rotorcraft,” Tech. Rep. ADS-33E-PRF, United States Army Aviation and Missile Command Aviation Engineering Directorate, March 2000, URL: <https://www.amrdec.army.mil/amrdec/rdrmr-se/tdmd/Documents/ads33front.pdf>.

³⁰ Key, D., Blanken, C., Hoh, R., Mitchell, D., and Aponso, B., “Background Information and User’s Guide (BIUG) for Handling Qualities Requirements for Military Rotorcraft,” techreport SR-RDMR-AD-16-01, U.S. Army Research, Development, and Engineering Command, Dec. 2015, URL: www.dtic.mil/dtic/tr/fulltext/u2/1000418.pdf.

³¹ Smeur, E., Hoppener, D., and De Wagter, C., “Prioritized Control Allocation for Quadrotors Subject to Saturation,” *International Micro Air Vehicle Conference and Flight Competition (IMAV)*, 2017, pp. 37–43, URL: http://www.imavs.org/papers/2017/51_imav2017_proceedings.pdf.

³² Johansen, T., Fossen, T. T. A. J., and Fossen, T. I., “Control Allocation – A Survey,” *Automatica*, Vol. 49, 2013, pp. 1087–1103, DOI: 10.1016/j.automatica.2013.01.035.

³³ Harkegard, O., “Efficient Active Set Algorithms for Solving Constrained Least Squares Problems in Aircraft Control Allocation,” *41th IEEE Conference on Decision and Control*, Dec. 2002, DOI: 10.1109/CDC.2002.1184694.